A study of catalytic metals and alkaline metal oxides leading to the development of a stable Ru-doped Ni Dual Function Material for CO_2 capture from flue gas and in-situ catalytic conversion to methane

Martha A. Arellano Treviño

Submitted in partial fulfillment of the
requirements for the degree of
Doctor of Philosophy
in the Graduate School of Arts and Sciences

COLUMBIA UNIVERSITY
2020

ABSTRACT

A study of catalytic metals and alkaline metal oxides leading to the development of a stable Ru-doped Ni Dual Function Material for CO_2 capture from flue gas and in-situ catalytic conversion to methane

Martha A. Arellano Treviño

Atmospheric CO_2 concentrations are at their highest level on record. Scientific evidence has demonstrated a direct correlation between the rise of CO_2 levels and an increase of the global median temperature (~1°C higher than compared to the pre-industrial revolution times) due to the greenhouse gas effect. The change in climate due to this rapid increase of CO_2 levels is already negatively affecting our ecosystem and lives, with unpredictable consequences in the future.

The main source of anthropogenic CO_2 emissions is attributed to the combustion of fossil fuels for energy production and transportation. Global indicators signal that carbon-intensive fuels will continue to be utilized as a main energy source despite the rising implementation of renewable energy sources. In order to curb CO_2 emissions, several carbon dioxide capture, utilization and sequestration (CCUS) technologies have been suggested. The current state-of-the-art CO_2 capture technology utilizes toxic and corrosive aqueous amine solutions that capture CO_2 at room temperature but require heating above the water boiling point temperatures to separate CO_2 from the amine solution; the latter of which is to be recycled. Once the CO_2 is purified, it is necessary to transport it to its sequestration site or an upgrading processing plant. These are complicated schemes that involve many energy-intensive and costly processes.

To address the shortcomings of these technologies, we propose a Dual Function Material (DFM) that both captures CO_2 and catalytically converts it to methane *in-situ*. The DFM consists

of a catalytic metal intimately in contact with an alkaline metal oxide supported on a high surface area carrier. The process operates within the flue gas at 320°C for both CO_2 capture and methane generation upon the addition of renewable H_2. The catalyst is required to methanate the adsorbed CO_2 after the capture step is carried out in an O_2 and steam-containing flue gas. Ruthenium, rhodium, and nickel are known CO_2 methanation catalysts, provided they are in the reduced state. All three were compared for performance under DFM flue gas conditions. Ni is a preferred methanation catalyst based on price and activity; however, its inability to be reduced to its active state after experiencing O_2-containing flue gas during the capture step was an outcome determined in this thesis. The performance of a variety of alkaline adsorbents ("Na_2O", CaO, "K_2O" and MgO) and carriers (Al_2O_3, CeO_2, CeO_2/ZrO_2 (CZO), Na-Zeolite-X (Na-X-Z), H-Mordenite Zeolite (H-M-Z), SiC, SiO_2 and ZrO_2-Y) were also studied. Selection of the best materials was based on CO_2 capture capacity, net methane production and hydrogenation rates that were evaluated with thermogravimetric analysis and in fixed bed reactor tests.

Rh and Ru DFMs were effective methanation catalysts with Ru being superior based on capture capacity, hydrogenation rate and price. Ru remained active towards methanation even after exposure to O_2 and steam-containing simulated flue gas. Alkaline adsorbents, in combination with reduced Ru, were tested for adsorption and methanation. Ru – "Na_2O"/Al_2O_3 DFMs showed the highest rates for methanation although CaO is also a reasonable candidate with slightly lower methanation kinetics. To date, we have demonstrated that γ-Al_2O_3 is the most suitable carrier for DFM application relative to other materials studied.

The Ni-containing DFM, pre-reduced at 650°C, was highly active for CO_2 methanation. However, the hydrogenation with 15% H_2/N_2 is completely inactive after exposure to O_2 and steam, in a flue gas simulation, during the CO_2 capture step at 320^{o}C. This thesis reports that small

amounts of precious metal (≤ 1% Pt, Pd or Ru) enhance the reduction (at 320°C) and activation of Ni-containing DFM towards methanation even after O_2 exposure in a flue gas. While ruthenium is most effective, Pt and Pd all enhance reduction of oxidized Ni.

Another objective of this thesis was to investigate whether a portion of the Ru, at its current loading of 5%, could be replaced with less expensive Ni while maintaining its performance. The findings show that the main advantage of the presence of Ni is a small increase in CO_2 adsorption and increase in methane produced, at the expense of a lower methanation rate. Extended cyclic aging studies corroborate the stable performance of 1% Ru, 10% Ni, 6.1% "Na_2O"/Al_2O_3.

Characterization methods were used to monitor physical and chemical changes that may have occurred during aging studies. Measurements of the BET surface area, H_2 chemisorption, XRD pattern, TEM images and STEM-EDS mapping were utilized to study and compare the structural and chemical changes between fresh and aged Ru doped Ni DFM samples. While similar BET surface areas were observed for the fresh and aged samples, some redispersion of the Ru and Ni sites was confirmed via H_2 uptake and the observed decreases in Ru and Ni cluster size in the aged sample in comparison to the fresh. XRD patterns confirm an almost complete disappearance of the NiO_x and RuO_x species and the appearance of catalytically active Ru^0 and Ni^0 peaks on the aged sample compared to the fresh one. Further details of these methods, findings and conclusions are described in this thesis.

Table of Contents

List of Figures

List of Tables

Acknowledgements

I would like to express my heartfelt appreciation to my PhD advisor and life mentor Prof. Robert Farrauto. His work ethic and passion for catalysis have been my guiding star during all these years. Ever since he gave me the opportunity to work in his research group, his unconditional support through the ups and downs of my PhD gave me the confidence I needed to give the best of me and succeed in this journey.

I give my sincere thanks to my committee members Prof. Jingguang Chen, Prof. Alissa Park, Prof. Ngai Yin Yip, and Dr. Michel Deeba for their time and help with my research throughout the years. I would also like to thank Prof. Edward Leonard for his career and life counsel during the past 8 years. I appreciate the opportunity he gave me when I was still an undergrad to come to Columbia for the first time and do an internship in his lab. This chance changed my life for the best and I will forever be in debt with him.

Many thanks to my sponsors. The Mexican Science and Technology Council (CONACYT), the Fulbright Scholarship and AngloAmerican Platinum for their generous financial support on my graduate studies.

Ever since I came to Columbia, I've had the opportunity to work with some wonderful people. I would like to especially thank Dr. Melis Duyar for her friendship and guidance during my PhD. She's been an inspiration for me, and it's been an honor to continue working on the advancement of the DFM project that she started. I would also like to acknowledge the former PhD students in our group: Dr. Ashley Wang, Dr. Angela Zheng, and Dr. Emi Leung for their friendship, mentorship and companionship throughout my PhD journey. I would like to thank all the former and present students that have collaborated with me, especially: Chae Jeong-Potter, Nisarg Kanani, Malia Libby, Nicky He, Amanda Huang, Brandong Xie, Rees Chang, Arvind

Ramachandran, Xiaoxuan Teng and Laura Proaño. Thank you all for sharing my passion for this project, for your hard work, creativity, friendship and for your time and dedication.

Many thanks to my Columbia friends, specially to Ricardo Esparza, my best friend for the past 3 years. Thanks to Ken Sinclair, James Doss-Gollin, Yash Amonkar, Anas Alkhani, Atishu Jain, Elaine Gomez, and Constantine Spanos for all the shared moments, the happy and stressful ones, for all the plans, the drinks, and the many experiences lived together.

I would also like to thank my lifelong friends, specially my best friend Marifer Loya, that has been my constant for 22 years, for always being there for me, my biggest cheerleader and warmest friend. To my college friends Mariana Moreno and Jared Martínez, for their constant support. My dearest friends Ángel García, Lauren Oliver, Mariana Basilio, Rianna and Alex Leighton, that have made my experience in NYC an unforgettable one.

A special thanks to Adam Atia, for being there for me during the arduous last year of my PhD, specially the last couple of months of thesis writing. For keeping me sane, focused and motivated. For his kind heart, for being my emotional support and for his infinite patience.

Finally, I would like to dedicate this thesis to my family. My sister Karla Arellano, who has been my biggest fan, my mother Martha Treviño, who is the voice inside my head and my father Carlos Arellano who is my biggest champion. Everything I do is to make them proud and if I have been able to come this far, it is because of their love.

To my family. My sister, Karla and my parents, Carlos and Martha

Chapter 1: Introduction

1.1. Motivation

Despite the rise in renewable power generation, the world's primary energy source is still based on combusting fossil fuels. According to the 2017 Global Energy and CO_2 Status report by the International Energy Agency (IEA) the global energy demand increased 2.1% in 2017 and almost three quarters (75%) of the rise was contributed by fossil fuels and a historically high 25% was provided by renewable sources. Global CO_2 emissions saw an overall increase of 1.4% but many countries like the United States saw a decline due to higher deployment of renewable energy sources and greater industrial conservation and efficiency. Of the fossil fuels, natural gas demand grew by 3% due to its availability and relatively low cost of supply. While most of it is used in the power sector, there is an increasing demand for its use in the industrial and construction sectors [1]. It is clear fossil fuels will continue to be used for combustion for the foreseeable future with the consequential generation of large amounts of CO_2.

According to the Intergovernmental Panel on Climate Change (IPCC) [2], sustained greenhouse gas emissions have caused impacts on the atmospheric and oceans systems. The increase of greenhouse gas emissions, linked with fossil fuel usage, will likely cause severe, long lasting and irreversible effects on the environment, ecosystems and humankind. It is, therefore, necessary to implement immediate actions to continuously limit and reverse greenhouse gas emissions to minimize any further exacerbation of climate change. Different scenarios have been modeled to estimate the costs of implementing low-carbon technologies to reach CO_2 atmospheric concentration targets for this century (2015 – 2100), and in all scenarios, carbon capture, utilization and storage (CCUS) technologies will play a crucial role in curbing greenhouse gas emissions at

the lowest mitigation costs. Several companies in countries such as Switzerland and Canada have emerged to provide solutions for CO_2 abatement through different CCUS schemes. For example, Inventys in British Columbia, Canada, offers services for CO_2 capture from stationary applications [3]. Carbon Engineering, also in Canada, and Climeworks in Switzerland both develop technology for direct air capture and utilization [4,5].

Current state-of-the-art CO_2 capture technology relies on toxic chemicals such as liquid amines, the most well-known being monoethanolamine (MEA), to scrub carbon dioxide from flue gas streams. Water is added to amine adsorbents due to their excessive corrosiveness and viscosity. Therefore, the process requires a large heat input, associated with the volatilization of water required to separate the CO_2 and the amine solution (MEA) the latter of which is recycled [6]. Direct air capture has several disadvantages as the source of CO_2 is very diluted (~400 ppm in air); the reactor bed needs to be large and requires an energy penalty to compress air into the system and maximize adsorption. These technologies face the disadvantage of low operating temperatures (25 – 120°C) where kinetics for CO_2 conversion to useful products are very slow, even in the presence of catalysts. Furthermore, a temperature swing is necessary to bring the captured CO_2 to higher temperatures for desorption and further processing (>200°C) [7–12].

Utilization of CO_2 as a reactant to generate useful products is an attractive approach that can offset the cost of capture if the resultant product has a significant market. It is important to clarify that the process would have to rely on H_2 generated from renewable energy sources (solar, wind, hydroelectric, geothermal, etc.) in order to approach carbon neutrality and sustainability.

Renewable energies like solar and wind are intermittent. Excess electrical energy must be stored during non-productive utilization periods. One way to use this excess renewable energy is to produce hydrogen via water electrolysis for future use. Even though renewable energy costs

have significantly dropped, the price of renewable hydrogen is still too high compared to large-scale industrial hydrogen production (from fossil fuels) [13]. An economic model developed by Glenk and Reichelstein [14] predicts that power-to-gas technologies will generate price competitive renewable H_2 in the next ten years. The model also predicts that policy incentives can make renewable hydrogen economically competitive as early as 2023 in places like Texas and Germany.

How can the increasing energy demand be satisfied in a sustainable and practical way, but also acknowledging that fossil fuels will likely continue to be the main source of energy in the foreseeable future? Furthermore, how can potential solutions achieve this with simple, energy-efficient processes and cost-effective materials? The objective of this thesis is to answer these questions by presenting the advances in the Dual Function Materials (DFM), initially developed by our research group in 2014 [15].

The Dual Function Material (DFM) is a dispersed alkaline CO_2 adsorbent, with a methanation catalyst both of which are supported on a high surface area carrier. DFM both captures CO_2 and catalytically converts it to methane (CH_4) in a single reactor at the same temperature. Taking for example an air-fired natural gas power plant, DFM would be placed downstream of the pollution abatement technology. In the first step, CO_2 would be captured by the dispersed alkaline oxide on alumina producing a CO_2-free flue gas vented to the atmosphere. Once the material is saturated, in a second step (offline) renewable hydrogen is introduced to convert the adsorbed CO_2 to methane which is recycled to the power plant inlet, reducing CO_2 emissions and approaching carbon neutrality. Alternatively, the methane produced can be safely and cheaply stored and distributed to many locations through the natural gas pipeline network.

The uniqueness of this material lies in the synergistic relationship between its two components. Dispersed alkaline oxides behave very differently from their bulk material counterparts [16] since reactive chemisorbed CO_2 occurs rather than bulk carbonate formation. Heat released by the exothermic methanation reaction drives the endothermic CO_2 desorption from the adsorption sites to the catalyst sites via the spillover mechanism [17] to complete methanation of all the adsorbed CO_2 at the same moderate temperatures of 250 – 350°C. This technology does not require additional energy input as it uses the sensible heat of the flue gas. We envision the implementation of the DFM with at least two parallel swing reactors where H_2 is added to the CO_2 saturated reactor while a parallel reactor continues to capture CO_2 allowing continuous operation. In order to be functional in a real industrial application, the CO_2 capture and hydrogenation steps should have similar rates for continuous operation. Aging studies have demonstrated stable performance for over 50 cycles of CO_2 capture and hydrogenation [18].

Our previous published work explored the 5%Ru, 10%CaO/Al_2O_3 and 5%Ru, 6.1%"Na_2O"/Al_2O_3 systems for maximum CO_2 capture and methanation capacity [15,19] and also established the stability of the systems in cycle tests in a simulated flue gas [18,20]. We also reported the CO_2 capture capacity of different dispersed alkali adsorbents (CaO/Al_2O_3, reduced Na_2CO_3/Al_2O_3, reduced K_2CO_3/Al_2O_3 and MgO/Al_2O_3) [21]. One of the aims of this thesis is to better understand the CO_2 capture mechanism of these adsorbents as well as the kinetics of the CO_2 methanation when in direct proximity to a methanation catalyst, with a specific focus on Ru. Previously, all DFM studies were carried out for samples dispersed on Al_2O_3. Thus, we explored alternative candidate carrier materials for the DFM application: CeO_2 (HSA: high surface area and LSA: low surface area), CZO, Na-Zeolite-X (Na-X-Z), H-Mordenite Zeolite (H-M-Z), SiC, SiO_2 and ZrO_2-Y with the initial objective of studying and understanding the metal/adsorbent/carrier

interactions for CO_2 capture and methanation over different supports in search of alternatives to Al_2O_3 that might enhance the DFM process.

In previous studies, we presented the performance of different precious metals (Ru, Rh, Pt and Pd) as well as base metal catalysts (Ni and Co) tested at stoichiometric conditions for methanation activity (4:1 H_2 to CO_2 ratio) over a temperature range of 250 – 350°C [21]. The methanation activity of the metals in descendent order was Ru > Rh > Ni. From an economical point of view, the screening of these metals offers relevant information since we can compare the catalytic activity of expensive Rh ($114.11 USD/g)*, moderately priced Ru ($7.99 USD/g)* and inexpensive Ni ($0.01 USD/g)*. Ni is clearly the most preferred metal from an economical point of view provided it has acceptable performance.

Even though Pt and Pd were not good methanation catalysts by themselves, previous studies demonstrated that doping Ni catalysts with small amounts of these precious metals could boost nickel's methanation activity to compete with that of Ru [22]. Lowering the precious metal loading by substituting with a more economical catalyst like Ni, would mean substantial reduction of the DFM costs, provided the new alternative could retain activity and stability in simulated O_2-containing CO_2 capture conditions.

This thesis presents a detailed study of methanation kinetics displayed by Ru, Rh and Ni catalysts in concert with dispersed alkaline adsorbents supported on a variety of carriers for cyclic CO_2 capture and catalytic methanation. We also present the feasibility studies of precious metal doped Ni bimetallic catalysts for CO_2 capture and methanation at simulated flue gas conditions. Cyclic aging studies and characterization of the fresh and aged samples demonstrated stability of

* Price as of 7/14/19

the bimetallic system and the possibility of reducing the amount of precious metal loading while increasing CO_2 capture capacity and methane production.

1.2. Thesis structure

This thesis presents the evaluation of catalytic metals (Ru, Rh and Ni) and adsorbents (CaO, "Na_2O", "K_2O" and MgO) intimately dispersed on high surface area Al_2O_3 and other carriers. CO_2 capture capacity and hydrogenation kinetics of the adsorbed CO_2 were studied as the variables of interest. We also present the enhanced reducibility of NiO at lower temperatures by doping small amounts of precious metals (Ru, Pt or Pd) on Ni DFMs for application in O_2-containing CO_2 capture processes and subsequent methanation. The results presented will demonstrate the stable performance of a Platinum Group Metal (PGM)-promoted Ni-containing DFM when exposed to simulated flue gas conditions for over 20 cycles of aging. Characterization of the fresh and aged sample confirm the stability of the catalytic system.

Chapter 2 presents a comprehensive literature review that provides the scientific foundation of the rise of CO_2 levels in the atmosphere due to anthropogenic activity as well as its correlation to global warming. It also presents a study of the known CO_2 capture, storage and utilization technologies, their main advantages and shortcomings. This chapter also contains a short review of the current status of the hydrogen production utilizing renewable powered sources. Finally, this chapter explains in detail the DFM concept, the newly discovered improvement in performance and initial scale up feasibility is presented.

The experimental methodology of the work presented is detailed in chapter 3. A description of the material synthesis, experimental setup and process conditions are provided. Also presented is a description of the equipment utilized, data acquisition and analysis methods.

Chapter 4 presents the study of the proposed metal/adsorbent/carrier combinations for DFM by comparing their respective CO_2 capture capacity, methanation kinetics and overall methane production. A difference between CO_2 removal via a catalyzed methanation reaction vs a non-catalyzed desorption is shown using thermogravimetric analysis (TGA). Fixed or packed bed reactor tests and TGA are used to highlight the influence of different catalysts (Ru, Rh and Ni), adsorbents ("Na_2O", CaO, "K_2O" and MgO) supported over different carriers (Al_2O_3, CeO_2, CZO, Na-Zeolite-X (Na-X-Z), H-Mordenite Zeolite (H-M-Z), SiC, SiO_2 and ZrO_2-Y). Standard characterization of all fresh materials is provided by measuring BET surface area and metal dispersion measurement is conducted with H_2 chemisorption at room temperature.

Chapter 5 presents the feasibility studies on various precious metals (Ru, Pt or Pd) in combination with Ni DFM catalysts. Fixed bed reactor tests present the limitations of Ni-only DFMs for O_2-containing flue gas conditions. TGA is performed on Ru or Pt-doped Ni/Al_2O_3 catalysts for isothermal reduction conditions at 320°C where enhanced NiO reducibility at lower temperatures is demonstrated due to the promoting effect of the precious metals. Fixed bed tests corroborate the promoting effect of Pt or Ru-doped Ni DFMs with Ru showing the greatest promotion consistent with TGA tests. Cyclic aging tests demonstrate stable performance of the Ru, Ni DFM using a simulated O_2 and steam-containing flue gas for the CO_2 capture step. Fresh and aged samples are characterized via TEM, XRD, H_2 chemisorption at 100°C and BET surface area measurements.

Chapter 6 presents the main conclusions from this thesis as well as the proposed future work to address the areas of opportunity to achieve commercialization of the DFM technology as well as other possible applications.

Chapter 2: Background and literature review

2.1. Rise of anthropogenic CO_2 emissions and correlation with climate change

The most recent Intergovernmental Panel on Climate Change (IPCC) report agrees that "*Climate change represents an urgent and potentially irreversible threat to human societies and the planet"* [23]. It also states that the mean global temperature has risen by 1°C since the industrial revolution (early 20th century), with some parts of the planet (like the north and south poles) seeing even a higher increase in their mean temperature. The report's goal is present the current political strategies and technologies available to curb climate change. The report includes models of different scenarios where we can reach the goal of limiting the mean global temperature rise to 1.5°C higher than that of pre-industrial times as well as scenarios of possible consequences to our environment if we fail to do so. The IPCC states that the effects of climate change are currently affecting biodiversity and life in all its forms around the world with devastating consequences, specially to island nations that are in great danger by the rise of the sea level and extreme weather conditions that can be attributed to this phenomenon.

There is a strong evidence that there is a direct correlation between the rising CO_2 concentration in the atmosphere and the rise of the mean global temperature. A study by Chen, et al. shows that CO_2 emissions contribute to about ~50% of the global temperature increase between the decades of 1990-2010, which corroborates this hypothesis [24]. The increase of the global temperature can be attributed by the strengthening of the greenhouse gas effect by the increase of the concentration of CO_2 in the atmosphere. The greenhouse gas effect is a natural and beneficial physical phenomenon that permits life on earth, without it, the surface temperature of our planet would be too cold to support a biodiverse ecosystem. Our atmosphere consists of a mixture of

gases, some of which are able to adsorb some of the infrared radiation that we receive from the sun, by this mechanism, the concentration of these "greenhouse" gases play a crucial role in the regulation of the temperature of our planet. In the late 1950s, Dr. Charles Keeling started measuring the concentration of these greenhouse gases from our atmosphere from the Mauna Loa Observatory in Hawaii. Soon after, other observatories around the world also started taking similar measurements. **Figure 2.1** presents the data collected over the years from several of these observatories which show an unequivocal increase of the concentration of CO_2, which is considered a greenhouse gas. Even though the CO_2 concentration is relatively small (411.5 ppm as of April 2019 [25]), it's been demonstrated that its radiative forcing impact is greater than the other greenhouse gases and for that reason it's been studied the most [26] .

The carbon cycle describes the natural mechanisms in which CO_2 concentrations are regulated in our planet. The main carbon reservoirs are the oceans, land and atmosphere where CO_2 can be found in diverse forms as part of the biomass, carbonaceous and fossil sediments as well as in its gas and ionic form. All of these carbon forms are in a delicate equilibrium that has been disrupted by anthropogenic activities since the industrial revolution where fossil sediments started to be utilized as fuels for power generation and for other human related activities. These fossil sediments have been burned at a rate faster than the natural carbon cycle mechanisms can assimilate them, therefore a net accumulation of carbon species in the atmosphere is observed.

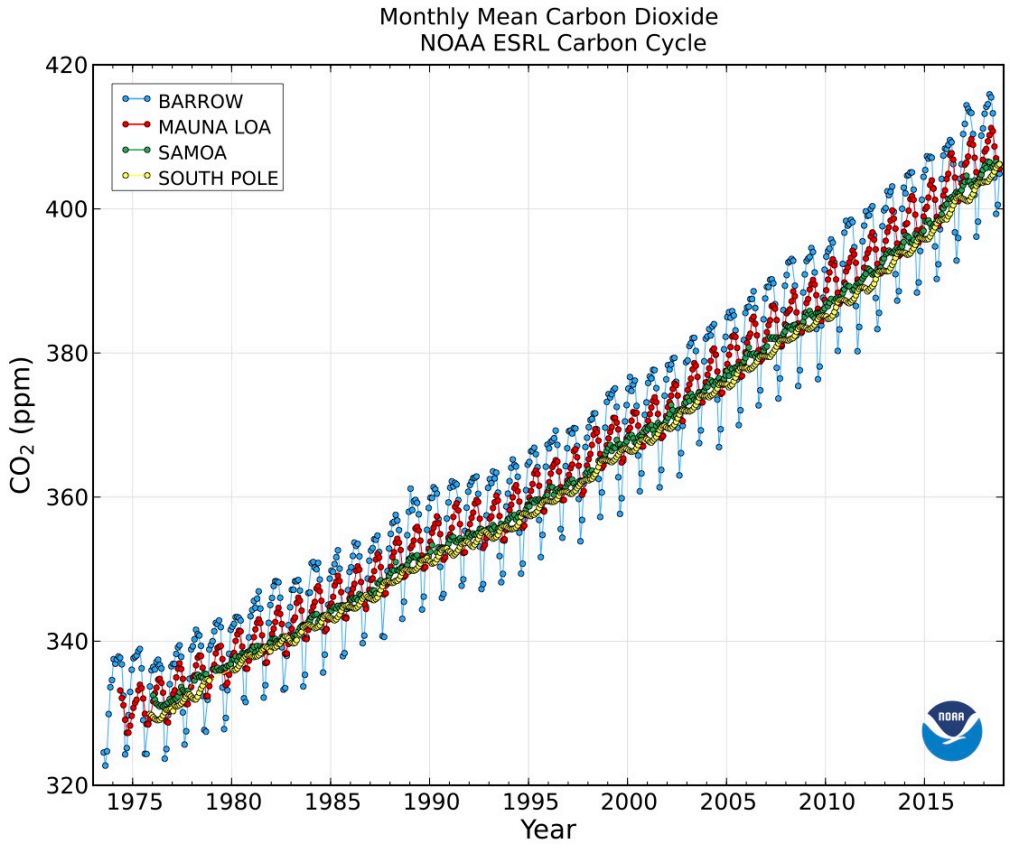

Figure 2.1. Monthly mean atmospheric CO_2 concentration in ppm determined from continuous monitoring programs at Barrow, Mauna Loa, Samoa and South Pole observatories [27].

2.2. CO_2 capture, sequestration and utilization technologies, their application and limitations

CO_2 capture technologies have been studied and developed in the past. Some motivations to separate CO_2 from a gas mixture are for purification of products when CO_2 is a byproduct or for sorption enhanced reactions (SER) methods for production of hydrogen via equilibrium-controlled reactions like integrated steam reforming of methane with water gas shift [28,29] taking advantage of Le Chatelier's principle. Capturing CO_2 in steam reforming (endothermic) allows operation at lower temperatures while for water gas shift (exothermic) adsorbing CO_2 allows operating at

higher temperatures where enhanced kinetics translates into reduction of reactor sizes. These are industrial driven reasons that allow cost reduction and improved quality control of the processes. However, recently the main motivation for capturing CO_2 from flue gas or post conversion industrial applications is to abate greenhouse gas emissions.

As mentioned previously, some of the major sources of anthropogenic CO_2 are the energy sector that rely on burning fossil fuels to produce electricity, the oil refineries, cement industry (decomposition of $CaCO_3$) , iron and steel industry, biogas purification via fermentation, diverse chemicals (ammonia, ethylene oxide, methanol, pharmaceuticals, etc.) production industries and transportation sector. These industries either utilize or produce CO_2 and therefore, are the perfect candidates to integrate some form of CO_2 separation technology [30]. CO_2 capture efforts can be classified in five major groups: oxy-fuel combustion, chemical looping process, direct air capture, pre-conversion capture and post-conversion capture.

Oxy-fuel combustion technology utilizes pure oxygen for combustion, which makes the process highly efficient with CO_2 and water as the only products. One of its advantages is that the flue gas has very high CO_2 concentration which is desired because it translates to a smaller reactor bed volume due to enhanced efficiency of capture. The main disadvantages rely on the high cost of cryogenic oxygen purification necessary for the combustion and the high percentage of CO_2 and vapor products is very corrosive.

Chemical looping combustion is a novel technology that utilizes metal oxides as oxygen carriers instead of using air or pure oxygen for combustion. In this process the metal oxide is reduced, providing oxygen that when in contact with fuel, combusts to produce energy, CO_2 and water. The reduced metal is then exposed to air to be re-oxidized and utilized again in a cycle of oxidation/reduction [31]. This technology has similar advantages as oxy-fuel combustion because

it produces very concentrated CO_2 flue gas that is easy to purify by simple water condensation. Chemical looping combustion overcomes the high cost of cryogenic oxygen purification and its main disadvantage is integrity of materials during recycle and that it's still in the early development stages.

Direct air capture is the process of capturing CO_2 from the atmosphere for subsequent purification and sequestration or future use instead of using (liberating) already sequestered CO_2 in form of fossil fuels, biomass or natural CO_2 reservoirs [32,33]. This is a relatively new concept that has gained more interest worldwide as the technology has been demonstrated in the laboratory, pilot plants and industrial scale [4,5,34]. The advantage of this technology relies on the future environmental benefit it will provide to remove CO_2 from the atmosphere that would otherwise take a very long time to be sequestered by natural means. The disadvantages of the process are the technical difficulties to adsorb such diluted amounts of CO_2 (~400 ppm) from air (which also has other contaminants that may have a negative impact on the adsorption efficiency) that require large reactor beds and an energy penalty to compress the air into the system to maximize the capture efficiency. Moreover, the regeneration of the adsorbents presents another disadvantage point since it relies on energy intensive temperature swing [13,34–37] since CO_2 capture is favored at a low temperature while separation from the adsorbent requires a higher temperature, not to mention that once the CO_2 is purified it has to be compressed and transported to a point of sequestration or reuse facility which is another drawback.

Pre-conversion capture occurs when CO_2 is an undesired intermediate byproduct of a larger desired reaction [30,31]. A clear example is the ammonia synthesis process. For this reaction, large amounts of hydrogen are needed. The H_2 is most widely provided via the integration of steam reforming of methane and water gas shift. CO_2 and H_2 are the main products of the integrated

process but hydrogen must be purified before reacting with the atmospheric N_2 in air to catalytically produce ammonia [38]. The most widely used method for CO_2 separation is the use of liquid absorbents like monoethanolamine (MEA). The amine scrubbing technology was developed in the early 20th century which makes it one of the most developed, tested and robust technologies for CO_2 capture. The technology is very well known and consists of a low vapor pressure aqueous amine solution that is put in contact with a CO_2 rich gas mixture at room temperature. The CO_2 forms a complex with the amine functional group that can be regenerated by a water vapor stripper unit which produces pure CO_2 that can be compressed and transported to a sequestration point or to be used as a reactant in a chemical process [6,39,40]. The main advantage of this technology is that it's already widely used and known but its disadvantages include the handling of corrosive, highly degradable amine solutions, the high energy penalty of the temperature swing necessary for decomposing the CO_2-amine complex and volatilization of the large amount of water present to minimize corrosion and provide fluidity and the compression and transportation of the pure CO_2.

Finally, post-conversion capture (also known as post-combustion capture when talking about energy production via burning fossil fuels in power plants) is the process of removing CO_2 from the final products of an industrial application like cement production, biogas purification, oil refining, ethylene production, etc. The same as pre-conversion capture, aqueous MEA is the most widely used solvent for post-conversion capture but many other technologies like membrane separation, hydrate-based separation, pressure swing adsorption, cryogenic separation and solid sorbents are also used [30,31,39,41–43].

Of the technologies mentioned before, solid sorbents are of particular interest. They can be categorized into low temperature (< 100°C) physisorbents, mid temperature (200 – 500°C)

chemisorbents and high temperature (> 500°C) bulk adsorbents [29]. CO_2 adsorption is an exothermic event that is thermodynamically favored at lower temperatures, physisorbents rely on the Van der Waals forces that exist between the porous sorbents' surface walls and the CO_2 molecules. These adsorbents also exploit the interaction between the strong quadruple moment of CO_2 molecules and the polar and ionic adsorbent sites [29,44]. Examples of low temperature physisorbents include zeolites, metalorganic framework compounds and activated carbons. These sorbents may be enhanced by modification with amine functional groups or other alkaline sites. The main advantages of physisorbents are their fast adsorption kinetics and high capture capacity. Desorption of CO_2 during regeneration is carried via temperature or pressure/vacuum swing cycles. The main disadvantages of these products are that their capture capacity rapidly decreases at temperatures higher than 100°C and also that they are not resistant to moisture, since water preferentially adsorbs on their surface over CO_2 so the feed gas should be a dry mixture [45].

Alternatively, there are high temperature bulk adsorbents that can reversible adsorb CO_2 at high temperatures. Some of the most common bulk adsorbents are alkaline metal oxides like CaO, MgO, BaO, Li_2O, etc as well as natural and man-made hydrotalcite materials (Mg-Al structures with different levels of carbonation and hydroxylation that determine their basicity and therefore, capture capacity) [45–47]. These materials have been used in their pure form or in combinations or promoted by different materials (like potassium, sodium, iron, gallium or zirconium, etc.) [48,49] to provide better cyclic stability and thermal resistance to sintering, which are some of the main problems that face these materials by working at high temperatures. CO_2 capture at high temperatures has been shown to promote endothermic equilibrium-dominated reactions like integrated methane steam reforming coupled with exothermic water gas shift and integrated gasification combined cycle (IGCC) [50]. The capture capacity of bulk adsorbents is very high

with initial fast kinetics of CO_2 capture on the surface of the material, followed by a slow mass transfer limited reaction to carbonate the core of the particles. Both the adsorption and desorption of CO_2 are favored at high temperatures close to the carbonate decomposition temperatures (> 500°C) [45,48].

Finally, we present the mid temperature CO_2 chemisorbents that can reversible adsorb CO_2 at temperatures ranging between 200 – 500 °C. Their CO_2 capture capacity is not as high as that of physisorbents or bulk adsorbents but they overcome some of the disadvantages of both since they can be designed for high CO_2 selectivity over water, N_2, H_2 and other gases with excellent cyclic stability since they don't suffer from sintering due to exposure to extremelly high temperatures [30,31,45]. These chemisorbents would be ideal candidates to remove CO_2 from flue gas or post-conversion applications since they preferentially adsorb CO_2 without pre-treating the feed to a specific temperature, pressure or moisture condition. Some examples of these materials are CaO and Na_2CO_3 promoted Al_2O_3 [16,51,52]. It has been reported that dispersed CaO and Na_2CO_3 on Al_2O_3 changes the adsorption mechanism compared to the bulk materials. In the case of CaO/Al_2O_3, at moderate temperatures, CO_2 chemisorbs onto the CaO sites without forming the strong carbonate bonds that appear in the bulk CaO. The weakly bound chemisorbed CO_2 can be adsorbed and desorbed at the same temperature (about 300°C) just by purging the system with N_2 or another inert CO_2-free gas mixture, eliminating the need for temperature swing or vacuum/pressure swing. Spectroscopic data shows no sign of carbonate bands forming of the surface of the CaO/Al_2O_3 material which explains the low temperature of desorption compared to the >700°C needed to decompose bulk $CaCO_3$ bonds [16]. In the case of Na_2CO_3 doped Al_2O_3, several studies confirm that by dispersing Na_2CO_3 on Al_2O_3, the Na_2CO_3 decomposition is initiated at much lower temperatures (as low as 150°C) both in air and inert atmospheres [53] relative to

the decomposition of bulk Na_2CO_3 (>600°C). The final composition of the material has been described as a sodium aluminate species that we designate "Na_2O"/Al_2O_3. Infrared studies report that CO_2 adsorbs into these Al—O---Na^+ sites as a combination of weakly bound monodentate and bidentate carbonates without forming strong carbonate bonds [17,54]. The weakly bound monodentate and bidentate carbonates are similarly decomposed at moderate temperatures (200 – 400°C) just by purging the system with a CO_2-free gas mixture [21].

Once the CO_2 is captured and purified it is necessary to establish a practical, safe and economic way to transport it. There are several ways to do this, from onshore/offshore pipelines, pressurized tanks that can be transported by land and sea, etc. All of these mediums have their own advantages, limitations, risks and costs associated to them. Most of the previously suggested transportation mediums work best by transporting CO_2 in its supercritical form, which is achieved at temperatures above 32.1°C and pressure above 72.9 atmospheres. This supercritical state also requires ultra-pure CO_2 with moisture levels or other contaminants below 500 ppm to ensure that the CO_2 remains in the supercritical one phase state. A dry composition is essential not only to maintain a single-phase during transportation but also to avoid corrosion of the pipelines (that are mostly made of carbon steel) and the pressurized containers [31].

There are several CO_2 storage or sequestration options available. Most of them make use of available and suitable geological sites. The most widely used and mature technology is the use of CO_2 for enhanced oil recovery (EOR). This technology consists of injecting supercritical CO_2 into the oil/fossil fuel reservoirs to facilitate their extraction [30,31]. The reason CO_2 works well for this process is that at its supercritical form it can be miscible with the oil and gas in the reservoirs decreasing their viscosity making the extraction more favorable. Enhanced oil recovery

is a well-known technology that has been practiced since the 1970s, but it mostly uses CO_2 extracted from natural reservoirs, which is undesirable from an environmental point of view.

Another CO_2 sequestration idea being explored more recently (early 2000s) are un-mineable coal beds. This is a way to recover trapped methane (natural gas) that exist naturally in these coal beds by injecting CO_2 in a similar way as EOR. This technology is already in practice in China, the USA, Canada and Japan's coal sediments [55–57]. These beds are excellent storage points, the same as old oil sediments, since they have very low permeability and therefore, have a low chance of CO_2 leaks. Saline aquifers also offer great potential for CO_2 sequestration. This technology is not as widely explored as EOR and coal bed injection, but there are several projects that are exploring the option in the North Sea, Canada and USA principally. This technology consists of injecting CO_2 in the deep aquifers that carry high salinity brine that has no use. The CO_2 can be diluted in these deep reservoirs where they would undergo a carbonation process trapping the CO_2 in the sediment instead of remaining in the aqueous solution [58]. It is important to mention that all of these sequestration technologies present a risk of leakage, however minor, which could defeat the purpose of removing CO_2 from the atmosphere.

CO_2 sequestration has many technical and logistical disadvantages, and even though it represents the only way to permanently remove CO_2 from the atmosphere, there's still not enough infrastructure and economic and policy incentives to make this technology viable. It is necessary to find more alternatives to make CO_2 capture more attractive, one of them is the idea to utilize CO_2 directly or as a building block to produce higher value products that can offset the costs associated to implementing CO_2 capture technologies.

CO_2 can be utilized by itself for many applications. To mention some, the EOR technology that has discussed previously, in the food industry to carbonate beverages, to preserve and package

foods, to extract flavors and scents, to decaffeinate coffee and as a refrigerant [30,59]. It can also be utilized in the chemical production industry as needed in the production of several commodity chemicals like urea, methanol and salicylic acid [60]. For all the previously mentioned applications, it is needed to have a pure CO_2 stream free of impurities, however, it is possible to utilize CO_2 present in flue gas to grow microalgae for biofuel production where both CO_2 and N_2 are nutrients for the microalgae. The benefit of this technology is that unlike biofuels made from crops, it doesn't pose a competition or threat to food demand. The main disadvantage resides in the large energy requirement of harvesting the algae and the need of big reactors for its large-scale production [61,62]. Another promising way to utilize and sequester CO_2 is to utilize it as a building block in the high-volume production of polymers. Polymers are long chains of carbon and other functional groups that are produced in massive quantities worldwide. They are very difficult to decompose so once the carbon is utilized for their production it can be fixated for centuries or thousands of years [63].

These CO_2 utilization processes would have to rely on energy generated from sustainable and near-zero carbon footprint renewable energy sources. Renewable energy sources like solar and wind are intermittent; therefore, excess electrical energy must be stored during non-productive times. Water electrolysis produces hydrogen which can be stored conveniently for further use. The concept of chemical energy storage has gained more popularity as a means to produce "clean" fuels using captured CO_2.

2.3. CO_2 catalytic upgrade

There are several technologies under investigation to convert CO_2 to useful products such as photochemical [64,65] and electrochemical [66,67] processes that are being widely studied

since they can offer a renewable energy source. However, their application appears to be limited due to their low conversions, poor product selectivity, lack of widespread infrastructure and therefore, have not yet been proved to be economically or technically feasible for scale up [60]. Another way to convert CO_2 to chemicals and fuels is via the catalytic conversion that offers the advantage of a more mature technology with well-established processes, scalability and well-known reactor design principles. There are many fuels that can be produced via CO_2 catalytic upgrade, for example, syngas ($CO + H_2$) production by CH_4 and CO_2 catalytic dry reforming. The syngas can be upgraded via Fischer-Tropsch process to higher value products and fuels. Other fuels that can be directly produced using CO_2 include methanol [68], formic acid [67] and methane [69] to mention a few.

Methane production using renewable hydrogen presents an attractive solution for energy storage. Even though H_2 is an energy carrier it has its drawbacks: it is highly flammable and difficult to transport. Currently there's a pilot plant in Germany, built by Audi that uses H_2 from renewable sources in combination with landfill gas rich in CO_2 to produce methane (CH_4) via catalytic hydrogenation. Methane can be integrated into the existing natural gas grid making it readily available to many [70,71]. CO_2 methanation is a highly exothermic reaction favored at lower temperatures with the right catalyst providing rapid kinetics in the low temperature regime of about 250 – 350°C and 1 atm. Even though conversion kinetics are faster at higher temperatures, competing reactions like reverse water gas shift become more thermodynamically favorable at T > 400°C with the production of undesired species like CO [69].

CO_2 methanation via the Sabatier reaction is a well know commercial technology that has been widely reported in the literature [7,9,9,11,46,72–74] and used for many years. Earlier studies

showed that Ru, Rh and Ni were the best methanation catalysts [21] consistent with the literature [8,9,78–83,10,46,65,69,74–77].

Differences in activity and stability have been reported for methanation catalysts supported on different carriers. Ceria has been studied over the years as a promising carrier for methanation catalysts demonstrating good activity, stability and promoting effect for both ruthenium and nickel catalysts [84–89]. Ceria – zirconia (CZO: $CeO_2 – ZrO_2$) as a carrier known for its good thermal stability, oxygen storage capacity and promoting effect on metal dispersion [90]. ZrO_2 was also considered since it has shown to be a promising carrier regarding activity and stability when impregnated with catalytic metals [84–86]. Zeolites are also viable candidates since they have high internal surface areas and can be ion-exchanged with alkaline cations as possible CO_2 adsorbents [91–95]. Recent studies shown that different TiO_2 phases (rutile and anatase) demonstrate different catalytic activities with Ru dispersed on rutile TiO_2 being the better catalyst at low temperatures [96,97]. Silica (SiO_2) was also studied as a reference for a high surface area inert carrier [80,98–101].

2.4. Dual Function Materials (DFM) for CO_2 capture and catalytic conversion

Anticipating the market need for CO_2 capture and conversion to useful products (utilizing renewable hydrogen) we present Dual Function Materials (DFM) as an alternative to current carbon capture utilization and sequestration (CCUS) processes. DFM both captures CO_2 and converts it to synthetic natural gas (CH_4) at the site of its use. It is composed of an alkaline chemisorbent and catalyst both supported on the same high surface carrier [15]. **Figure 2.2** presents a schematic description of the dual function material in operation. Flue gas (from power plants, boilers, compressors, etc.) is first treated for pollution abatement removing CO, HC and

NO_x. It then enters a packed bed reactor at 320°C, containing a DFM where on a first step CO_2 is selectively adsorbed on the alkaline adsorbent sites. On a second step, the adsorbed CO_2 is then hydrogenated also at 320ºC with renewable H_2 to produce CH_4 and H_2O. The heat released by the methanation reaction creates a synergistic effect that drives the CO_2 desorption from the alkaline adsorbent sites which spills over to catalytic sites to produce CH_4 (synthetic natural gas) + $2H_2O$ after each cycle [17]. After drying and compressing, the CH_4 can be recycled to the inlet for re-combustion or can be distributed and transported to other locations through the natural gas pipeline network. At least two parallel reactors act in tandem for continuous capture and conversion. Aging studies have demonstrated stable performance for over 50 cycles of CO_2 capture and hydrogenation using a 5%Ru, 6.1% "Na_2O"/Al_2O_3 DFM [18].

The main advantages of DFM over the other technologies presented in this chapter are:

1. Elimination of corrosive amines
2. Elimination of temperature and/or vacuum swing desorption
3. In-situ production of synthetic natural gas (CH_4), which can be recycled for re-combustion. This decreases the volume of natural gas imported for the plant. Furthermore, the process approaches a carbon neutrality
4. Using excess renewable energy to produce synthetic natural gas (or methane) is a way to safely and cheaply store and distribute renewable fuels to many locations through the natural gas pipeline network.
5. No CO_2 purification or transportation is needed since the process is carried out at the site of CO_2 generation
6. The exhaust from a natural gas power plant provides the temperature required for the process (320°C) eliminating any the need for external heat input.

7. Ambient air containing ~400 ppm CO_2 is used for combustion and therefore its CO_2 is processed with the DFM technology eliminating stand-alone equipment for direct air capture.

The main drawbacks of DFM are:

1. The need for economical renewable H_2 and its infrastructure
2. Most likely, the excess H_2 required to ensure complete methanation will have to be separated from the natural gas produced to be reused
3. The DFM contains an expensive precious metal (Ru at ~ $8/g) which can be leased and recycled
4. Parallel reactors are needed for continuous operation. It is conceivable to implement a rotating bed design with two chambers; one chamber being hydrogenated while the other is capturing CO_2
5. Traces of NO_x not removed during upstream SCR will likely have to be adsorbed prior to the flue gas entering DFM

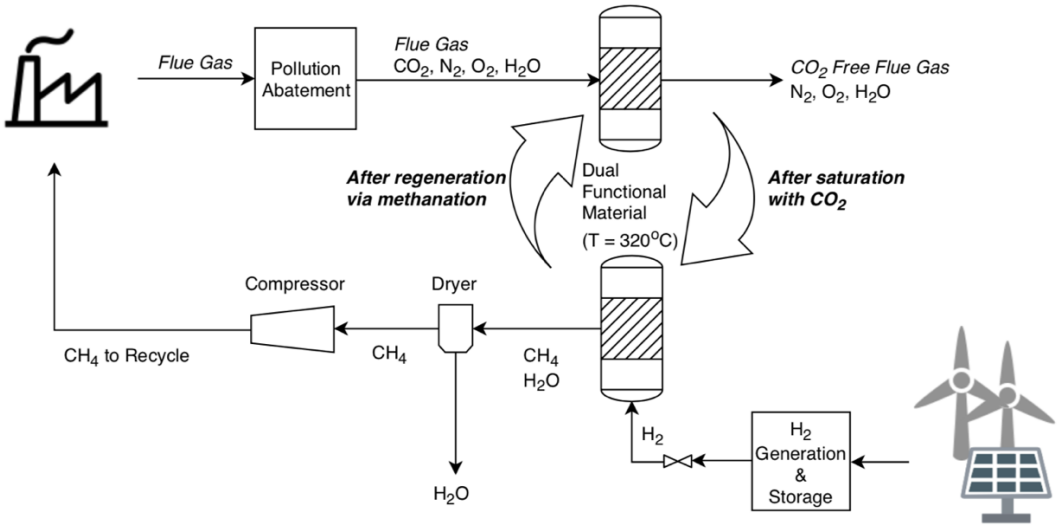

Figure 2.2. Schematic description of the proposed DFM process flow diagram

Ruthenium has unique redox properties that allow it to rapidly reduce to its catalytically active state after exposure to an oxidizing environment (such as power plant flue gas) during the CO_2 capture step [16]. While Ni is the most widely used methanation catalyst commercially, when exposed to an oxidizing environment during the CO_2 methanation, it dramatically and steadily loses activity over time [11]. Many research groups have studied Ni-containing DFMs but in all these studies the capture step is conducted in an O_2-free environment [102–105]. Several precious metals like Pt, Pd and Ru are known to dissociate H_2 molecules [106,107], rendering them stronger reductants for NiO and CuO, lowering the oxide reduction temperature [8,22,101,108–111]. Success by promotion with small amounts of precious metals (Pt and Ru) would make Ni-containing DFMs suitable for O_2-containing flue gas applications. This would mean a significant improvement in the DFM economics.

Previously, we reported the CO_2 capture capacity of different dispersed alkali adsorbents (CaO/Al_2O_3, reduced Na_2CO_3/Al_2O_3, reduced K_2CO_3/Al_2O_3 and MgO/Al_2O_3) [21]. The dispersed

carbonates, in the presence of a catalyst, are hydrogenated (producing CH_4) to what we assume are "Na_2O" /Al_2O_3 and "K_2O"/ Al_2O_3, respectively [6-8]. Quotation marks (" ") are used since their exact chemical composition has not yet been confirmed by XRD or other characterization methods. These dispersed adsorbents are acceptable for DFM applications since they reversibly chemisorb CO_2 at moderate temperatures (200 – 400°C) allowing for catalytic methanation [21].

The selection of Ru, and the rejection of Ni alone for O_2-containing flue gas is a critical part of this thesis. A new bimetallic catalyst composed of Ni with Ru has been demonstrated for use in DFM in O_2-containing flue gas. The selection of reduced Na_2CO_3 on Al_2O_3 compared to other alkaline adsorbents and carriers is also a focal point of this thesis. Characterization of fresh and aged materials is also included for completeness.

Chapter 3: Experimental Methodology

3.1. Material synthesis

3.1.1. 5%Ru, Adsorbents/Al_2O_3

"Na_2O", CaO, "K_2O" and MgO adsorbents were prepared by incipient wetness impregnation using aqueous precursor solutions of Na_2CO_3 (Sigma Aldrich, USA), $Ca(NO_3)_2$ (Sigma Aldrich, USA), K_2CO_3 (Sigma Aldrich, USA) and $Mg(NO_3)_2$ (Sigma Aldrich, USA) respectively impregnated on γ-Al_2O_3 (SBA-150, BASF, USA) powder. Adsorbents were then dried at 140 °C for 2h and calcined in air at 400°C for 4h. After calcination and H_2 reduction, the achieved loadings of adsorbents were 6.1% "Na_2O"/Al_2O_3, 7.1% "K_2O"/Al_2O_3, 10% CaO/Al_2O_3 and 10%MgO/Al_2O_3. Quotation marks (" ") are used since their exact chemical composition has not yet been confirmed by XRD or other characterization methods.

Ruthenium (III) nitrosyl nitrate (Alfa Aesar, USA) was impregnated onto the adsorbents supported on γ-Al_2O_3 to achieve the desired metal loading (by weight) of 5%Ru. All materials were dried in air at 120 °C for 2h and calcined in air at 250°C for 2h. The pre-reduction step was performed in situ at 320°C with 10-15% H_2/N_2 to generate the active catalytic metal and convert any remaining carbonates and nitrates to their respective oxides. Calcination temperatures were limited to 250°C to avoid formation of volatile RuO_x.

3.1.2. Metal, 6.1% "Na_2O"/Al_2O_3

Catalyst precursor salts were impregnated onto the 6.1% "Na_2O"/Al_2O_3 adsorbent, to achieve the desired metal loading (by weight) of 0.5%Rh and 10% Ni respectively. Samples were prepared using Rhodium (III) nitrate (BASF, USA) and Nickel (II) nitrate (Alfa Aesar, USA) respectively. All materials were dried in air at 120 °C for 2h and calcined in air at 500 °C for 2h. The pre-reduction step was performed in situ at 320°C with 10-15% H_2/N_2 to generate the methanation active Rh catalytic metal and convert any remaining carbonates and nitrates to their respective oxides. However, for oxides of Ni it was necessary to pre-reduce at 650°C with 10-15% H_2 to generate methanation active Ni metal.

3.1.2. 5%Ru, 6.1% "Na_2O"/Carriers

Zirconium (IV) oxide-yttria stabilized (ZrO2-Y) (Sigma Aldrich, USA), Na-Zeolite-X (Na-Z-X) and H-Mordenite Zeolite (H-M-Z) (Riogen, NJ, USA), Silicon Carbide (SiC) (SiCat, Germany), CeO_2/ZrO_2 (CZO) (BASF, NJ, USA), high surface area CeO_2 (CeO_2-HSA) and low surface area CeO_2 (CeO_2-LSA) provided by the University of Udine, Italy and Silica (SiO_2) (Sigma Aldrich, USA) were impregnated via the incipient wetness method using aqueous precursor solutions of Na_2CO_3 (Sigma Aldrich, USA) and Ruthenium (III) nitrosyl nitrate as previously explained (section 3.1.1.) to achieve 5%Ru, 6.1% "Na_2O" loadings into the different carriers.

3.1.3. 10% Ni, 6.1% "Na_2O"/Al_2O_3 samples doped with Ru, Pd or Pt

The 6.1% "Na_2O"/Al_2O_3 adsorbent was prepared by incipient wetness impregnation using an aqueous precursor solution of Na_2CO_3 (Sigma Aldrich, USA) impregnated on γ-Al_2O_3 powder (Sasol, TH100, Germany) using the same conditions explained in section 3.1.1.

Nickel (II) nitrate (Alfa Aesar, USA) was impregnated via incipient wetness onto the 6.1% "Na_2O"/Al_2O_3 adsorbent. The material was dried at 120 °C for 2h and calcined in air at 500°C for 2h producing a 12.4% NiO loading, which is equivalent to 10% Ni after reduction in hydrogen. For the purpose of identifying samples, they were labeled using the weight loading percentages of the most reduced state of the metal (10%) even when a Ni/NiO_x mixture is present in the sample after reduction in hydrogen at 320°C.

Finally, salts of Ruthenium (III) nitrosyl nitrate (Alfa Aesar, USA), Palladium (II) nitrate (BASF, Iselin, NJ) or a water-soluble amine Pt salt (BASF, Iselin, NJ) respectively were impregnated onto 10%Ni, 6.1% "Na_2O"/Al_2O_3 to reach a final loading of x% wt. Ru, Pd and Pt (x = 0.1, 1). All catalysts were dried at 120 °C for 2h and calcined in air at 500°C for 2h except for the Ru samples calcined at 250°C for 2h to prevent the volatilization of RuO_x. All samples were pre-reduced *in-situ* with 15%H_2/N_2 for 2.5 h (pre-reduction temperatures for samples are indicated in section 3.3.2.)

3.2. Thermal Gravimetric Analysis (TGA) tests

3.2.1. Hydrogenation kinetics and CO_2 capture capacity measurements

50 mg of powder materials were placed in an alumina crucible and underwent a cycle of CO_2 adsorption/hydrogenation in a NETZSCH TG209 F1 Libra instrument. All samples received *in-situ* pre-reduction at 320°C in 13.26% H_2/N_2 (Standard Ambient Temperature and Pressure (SATP): 60 ml/min) for 6h. CO_2 adsorption was conducted at 320°C with 6.66% CO_2/N_2 (SATP: 60 ml/min) for 30 min. The weight increase represents the amount of CO_2 adsorbed. This was followed by a 10 min N_2 purge, and then a catalytic hydrogenation step using 13.26% H_2/N_2

(SATP: 60 ml/min) for 6 h at 320°C. The weight decrease (removal of adsorbed CO_2) after the addition of H_2 gives a relative measure of weight loss associated with CO_2 converted to CH_4 or simply desorbed unreacted. Confirmation of the products was determined in fixed bed reactor tests using the Enerac analyzer.

The rate (slope) of CO_2 weight loss due to either hydrogenation or unreacted CO_2 desorption is calculated in mg/min after the first 5 min of 13.26% H_2/N_2 exposure. The time necessary to hydrogenate/desorb all the captured CO_2 is also presented. The relative rate of desorption is calculated by dividing all the hydrogenation rates by the slowest rate presented in the table, therefore making it the reference rate = 1.

3.2.2. Oxidation and reducibility capacity measurement

30 mg of powder 10%Ni/Al_2O_3 was placed in an alumina crucible and underwent a cycle of oxidation/reduction using a NETZSCH TG209 F1 Libra instrument. The initial sample was pre-reduced at 650°C in 15% H_2/N_2 (SATP: 60 ml/min) for 6h. The sample was exposed to 4.5% O_2/N_2 (SATP: 60 ml/min) at 320°C simulating the flue gas capture for 20 min. The weight increase is the extent of oxidation. This was followed by a 10 min N_2 purge (SATP: 20 ml/min), followed by the addition of 15% H_2/N_2 (SATP: 60 ml/min) for 6 h at 320°C. The weight decrease gives a relative measure of the extent of reduction of the oxidized sample.

3.2.3. Effect of Platinum Group Metal (PGM) doping on NiO_X redox properties

The tests were conducted using a 1%wt. loading of platinum group metals (Ru and Pt) impregnated on 10% Ni/Al_2O_3. 30 mg samples were placed in an alumina crucible and were heated to 320°C and 1 atm at a rate of 10 K/min in inert N_2 (SATP: 20 ml/min). They were then exposed

to a reducing environment with a 13.26% H_2/N_2 stream (SATP: 60 ml/min). The weight loss was recorded after constant weight was achieved.

3.3 CO_2 capture and methanation with different compositions of DFMs

3.3.1. Screening of DFMS with different catalysts, adsorbents and carriers using the Quantachrome unit as a fixed bed reactor

The basic Quantachrome equipment is designed for BET surface area measurements, quantification of dispersed metal availability by H_2 or CO chemisorption, and temperature programed reduction and desorption (TPR/TPD). We have modified it as a reactor for CO_2 capture and subsequent catalytic hydrogenation.

The samples (100 mg of powder) were placed in a u-shaped quartz tube fixed bed ChemBET Pulsar TPR/TPD unit (Quantachrome) reactor to test for CO_2 capture, followed by methanation upon hydrogen introduction. Temperature was controlled by a heating mantle surrounding the u-shaped reactor cell. The samples were first reduced overnight (12 h) at 320°C in 10% H_2/N_2 (SATP: 30 mL/min). This ensured that all the precursor salts decomposed to their reduced and active form. Only the Ru and Rh DFMs could be tested on the Quantachrome unit since the mantle that controls the temperature inside the reactor cell is limited to a maximum of 400°C. The NiO catalysts that require a pre-reduction temperature of > 500°C in H_2 [84–86] for complete reduction and therefore, had to be evaluated in a packed bed reactor.

Each sample was then exposed to a 10% CO_2/N_2 mixture (SATP: 30 mL/min) at 320°C for 40 min for the CO_2 capture step. The methanation step followed, with 10% H_2 /N_2 (SATP: 30 mL/min) introduction for 1 h. Three consecutive cycles (CO_2 capture + N_2 purge + methanation)

were performed and the results averaged. Gas compositions at the exit of the reactor were monitored using an Enerac portable emissions analyzer, capable of continuously monitoring CO_2, CH_4 and CO concentrations (1 second sampling time). The Enerac analyzes post combustion gas mixtures using an infrared detector as well as an electrochemical cell for O_2 detection. Its measurement accuracy is stated as 96%. No CO was detected in any tests. A blank test was performed with an empty reactor cell to record the carbon dioxide and methane baseline signals for accurate subsequent CO_2 and CH_4 measurements.

3.3.2. Packed bed reactor tests

1 g of powdered samples was tested in a packed bed reactor made of a quartz (O.D.=12.75mm, I.D.=10.5 mm and length=500mm). A microthermal furnace (MTSC12.5R-.75 × 18−1Z, Mellen, USA) surrounded the reactor tube with temperature feedback control from a K-type thermocouple (Omega, USA) at the inlet of the catalytic bed. Compressed gases were mixed at designed flow rates with mass flow controllers (MKS Instruments, USA). Steam was introduced to the feed gases by injecting water with a syringe pump (Cole-Parmer, USA). The water was pre heated to 125°C inside the reactor feed tube wrapped with heating tape. The steam from the feed or from the water produced during methanation was condensed in an ice bath placed at the exit of the reactor. An Enerac 700 analyzed the dry gas composition of CH_4, CO, CO_2 and O_2 every second. The Ru-containing samples were pre-reduced at 320°C and 1 atm for 150 min with 15%H_2/N_2 at a total flow rate of SATP: 200 ml/min (Gas Hourly Space Velocity (GHSV): 8000 h^{-1}). Pt and Pd-containing samples were pre-reduced at 500°C and 1 atm, at similar flow rate conditions. The 10%Ni, 6.1% "Na_2O"/Al_2O_3 samples were reduced at 650°C and 1 atm, at similar flow rate conditions. After pre-reduction, the samples were tested for isothermal CO_2 adsorption

and methanation cycles at 320°C and 1 atm. The 320°C temperature was necessary to simulate the continuous operation of the DFM with O_2-containing flue gas. **Figure 3.1** presents a schematic description of the reaction operation conditions.

The 4-min N_2 purge is needed both before and after CO_2 adsorption and methanation to avoid contact of possible explosive H_2 and O_2 in the catalytic bed. Each sample was tested for 3 consecutive cycles (1 cycle = CO_2 capture step + N_2 purge + methanation step+ N_2 purge).

A blank test was performed with an empty reactor cell to record the carbon dioxide and methane baseline signals for accurate subsequent CO_2 and CH_4 measurements. The CO_2 flow rate (in ml/sec) vs time (sec) during CO_2 capture and CH_4 flow rate (in ml/sec) vs time (sec) during hydrogenation are plotted and the area under the curves measured using the data analysis software Origin (OriginLab Corporation).The area under the curve gives the amount of methane produced and the CO_2 captured in ml. **Figure 3.2A** shows an example of a characteristic CO_2 signal recorded during CO_2 capture step and the blank profile used to calculate the CO_2 captured. The averaged (over 3 cycles) and normalized (using an empty reactor as a baseline) CO_2 signals and CH_4 peaks (see **Figure 3.2B**) were used to calculate the amount of CO_2 adsorbed and methane produced by the samples by subtracting the area of the blank to the area of the sample.

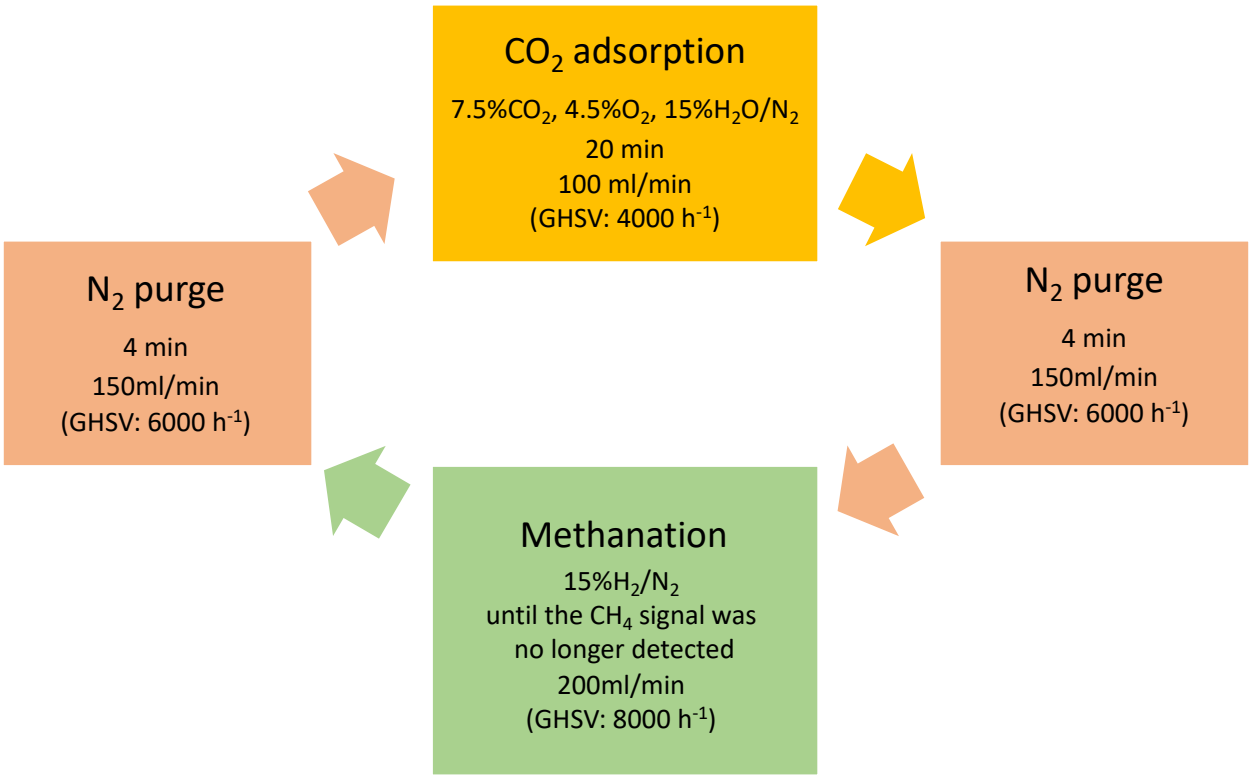

Figure 3.1. Schematic description of cyclic DFM operation. All steps conducted at 320°C and 1 atm. Volumetric flow rates corrected to Standard Ambient Temperature and Pressure (SATP: 25°C and 1 atm).

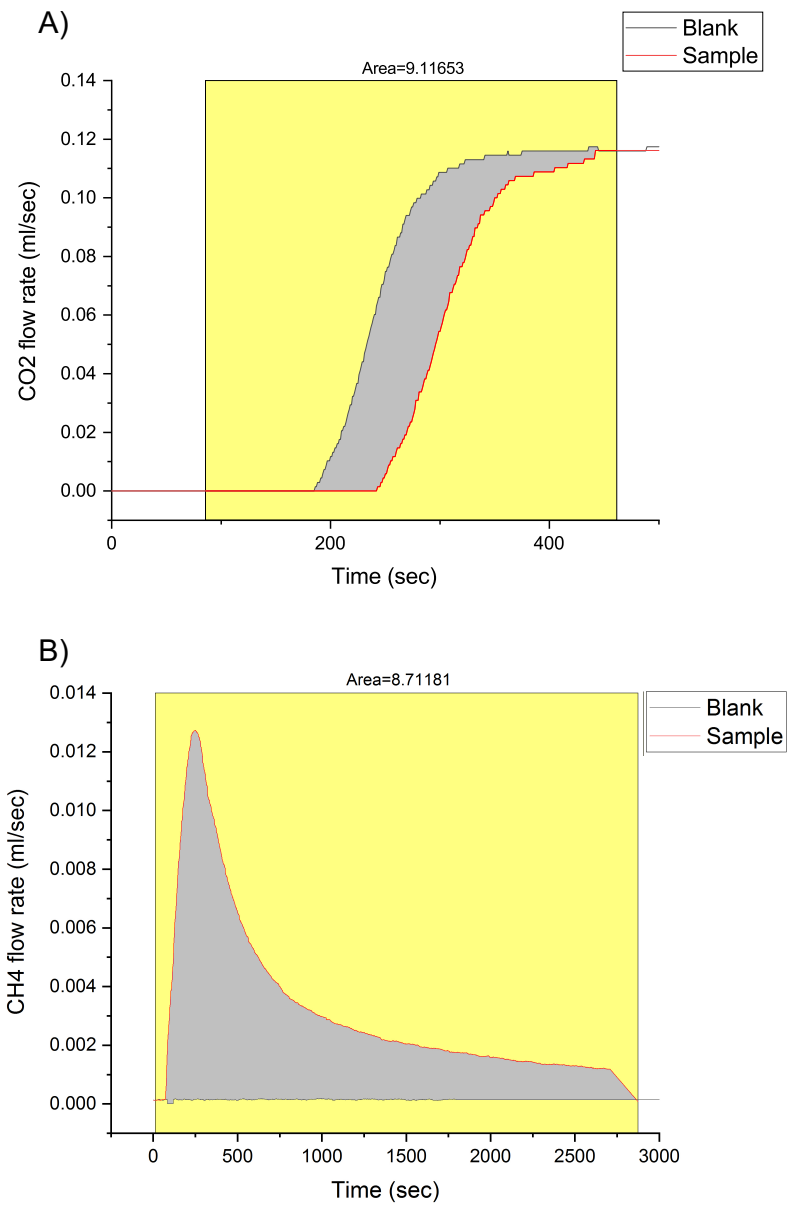

Figure 3.2. A) Characteristic CO_2 signal recorded during the CO_2 capture step in red compared to a Blank (empty cell) signal in black. The difference in areas represent the CO_2 captured by the sample (area in gray). B) Characteristic CH_4 peak recorded during the hydrogenation step in red compared to a Blank (empty cell) signal in black. Area under the peak curve in grey represent the CH_4 produced by the sample.

3.3.3. Cyclic aging tests in O_2-containing simulated flue gas

The most promising DFM composition, based on CO_2 capture capacity and methane production rate (from packed bed reactor tests), was selected for 20 cycles of aging. The experimental procedure was described in section 3.3.2 The sample was pre-reduced at 320°C for 2.5 h with 15%H_2/N_2 (GHSV: 8000 h^{-1}) before the beginning of the first cycle. The schematic description of the cycles can be found in **Figure 3.1** with the only difference being that the methanation step time was fixed at 30 min.

3.5. Characterization

3.5.1. BET

A ChemBET Pulsar TPR/TPD unit (Quantachrome) was used to measure single-point BET surface area for fresh and spent DFM samples. First, the samples were degassed *in-situ* for 2 hours at 150°C and 1 atm to remove any moisture from the sample. Subsequently, the BET surface area was measured at 25°C and 1 atm. Three measurements were made for each sample.

3.5.2. H_2 chemisorption

H_2 chemisorption tests were performed using a ChemBET Pulsar TPR/TPD unit (Quantachrome). Ruthenium and rhodium metal dispersions were obtained at room temperature (25°C) after reduction in situ in 10% H_2/N_2 at 320 °C (SATP: 30 ml/min) for 12 h. It was assumed that stoichiometry for relative chemisorption is one H atom per Ru or Rh site.

Fresh and aged (after 20 cycles) 1%Ru, 10%Ni, 6.1% "Na_2O"/Al_2O_3 DFM powder samples were reduced *in-situ* in 10% H_2/N_2 at 320 °C (SATP: 30 ml/min) for 12 h. H_2 adsorbed/g of material was obtained at 100°C.

3.5.3. X-ray diffraction (XRD)

X-ray diffraction (XRD) patterns of the fresh and aged (after 20 cycles) 1%Ru, 10%Ni, 6.1% "Na_2O"/Al_2O_3 DFM were performed using a PANalytical XPert3 Powder XRD. Patterns of γ-Al_2O_3 (Sasol, TH100, Germany) powder as well as 1%Ru 6.1% "Na_2O" /Al_2O_3 and 10%Ni, 6.1% "Na_2O"/Al_2O_3 were also scanned for comparison. The XRD is equipped with Cu K-α radiation, and the diffraction data was obtained at $2\theta = 20° \sim 85°$ with a step size of 0.01.

3.5.4. Transmission Electron Microscopy (TEM) and Energy-Dispersive X-Ray Spectroscopy (EDS)

The transmission electron microscopy (TEM) image and energy-dispersive X-ray spectroscopy (EDS) mapping was conducted in a FEI Talos F200X TEM instrument operating at 200 kV. The scanning transmission electron microscope (STEM) EDS mapping was obtained with the size of the selected Condenser 2 aperture at 50 μm and the spot size was 9. The EDS scans were acquired by Super X-EDS system.

The samples were prepared by depositing one droplet of the DFM colloidal suspension in isopropanol onto copper grids coated with a thin carbon film.

Chapter 4: Study of various catalytic metals/alkaline adsorbents/ carrier combinations for DFM: comparison of capture capacity and rates of reaction

The results presented in this chapter have been published in M.A. Arellano-Treviño, Z. He, M.C. Libby, R.J. Farrauto, Catalysts and adsorbents for CO_2 capture and conversion with dual function materials: Limitations of Ni-containing DFMs for flue gas applications, J. CO_2 Util. 31 (2019) 143–151.

This chapters explores different catalytic metals (Ru, Rh or Ni) in combination with a variety of alkaline adsorbents ("Na_2O", CaO, K_2O and MgO) as candidates for DFM application. Materials such as CeO_2 (HSA: high surface area and LSA: low surface area), CeO_2/ZrO_2 (CZO), Na-Zeolite-X (Na-X-Z), H-Mordenite Zeolite (H-M-Z), SiC, SiO_2 and zirconium oxide-yttria stabilized (ZrO_2-Y) were investigated as possible alternatives to alumina as a DFM carrier. All samples were tested in a fixed bed reactor to quantify the extent and rate of methane generation. Complementing fixed bed testing, thermogravimetric analysis (TGA) was used to evaluate the extent of CO_2 adsorption and rate of catalytic methanation.

4.1. Catalyzed vs. non catalyzed effect on CO_2 adsorption and hydrogenation/ CO_2 desorption rates.

Figure 4.1 presents the thermogravimetric and calorimetric profiles of the effect of catalyzed vs non-catalyzed CO_2 adsorption and catalytic hydrogenation or thermal CO_2 desorption rates (the experimental conditions are explained in detail in section 3.2.1). A weight gain is noted at the initiation of CO_2 adsorption on 6.1% "Na_2O"/Al_2O_3 (blue profile top half of **Figure 4.1**)

with an exothermic event (blue peak at t=0 lower profile in **Figure 4.1**).This is consistent with thermodynamics of adsorption processes and previous studies [19]. The amount of CO_2 adsorbed (blue profile in **Figure 4.1**) is less than when combined with reduced Ru which also adsorbs CO_2 (top red curve with the associated exotherm lower half of **Figure 4.1**).

Upon the addition of H_2, the adsorbent alone (in blue) produces no CH_4 (verified by the lack of exotherm associated with hydrogenation and external product analysis) but shows a very slow weight loss indicative of the thermal desorption of chemisorbed CO_2. The slow desorption (blue profile in Figure **4.1**) is complete after 360 minutes. In contrast, the rate of hydrogenation to CH_4 (as noted by the weight loss for the Ru catalyzed DFM), was considerably faster and complete in 36 minutes (red profile in **Figure 4.1**) and corroborated by the exothermic peak and analysis in fixed bed reactor tests. The reaction produces 1 mol of CH_4 and 2 moles of H_2O (1) leaving empty Ru sites free to accept CO_2 which spill over from the adsorbent to the Ru sites allowing for methanation. This postulated scheme is shown in equations 4.1, 4.2 and 4.3. Equation 4.3 is a repeat of equation 4.1. This mechanism has been furtherly corroborated by our *in-situ* DRIFTS studies. We report that CO_2 adsorbs onto Al—O---Na^+ (as bicarbonates and bidentate carbonates) with subsequent spill over to Ru sites for methanation upon the addition of H_2. Formate species were found to be the main reaction intermediates in methanation [17].

$$Ru\text{-----}CO_2 + 4H_2 \longrightarrow CH_4 + + 2H_2O + Ru \quad (4.1)$$

$$\text{“}Na_2O\text{”----}CO_2 + Ru \longrightarrow Ru\text{----}CO_2 + \text{“}Na_2O\text{”} \quad (4.2)$$

$$Ru\text{-----}CO_2 + 4H_2 \longrightarrow CH_4 + + 2H_2O + Ru \quad (4.3)$$

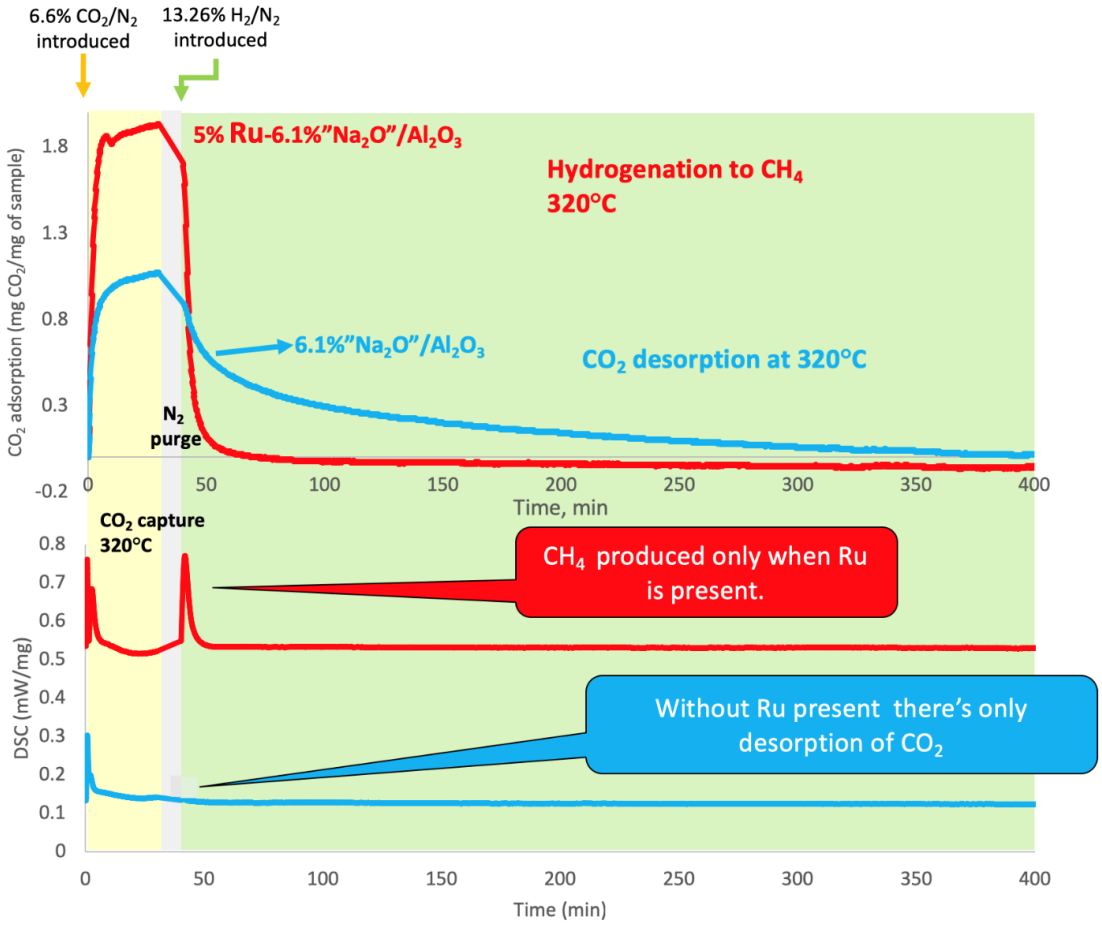

Figure 4.1. CO_2 adsorption and catalytic hydrogenation or thermal CO_2 desorption rates. Bottom 2 profiles are the DSC signals while the two top profiles are the mass profiles for 5%Ru, 6.1% "Na_2O"/Al_2O_3 (red) and 6.1% "Na_2O"/Al_2O_3 (blue). Adsorption feed gas was 6.6% CO_2/N_2 with hydrogenation initiated upon exposure to 13.26% H_2/N_2, both at 320°C.

4.2. Limitations of Ni-based DFMs at simulated flue gas CO_2 capture and conversion

4.2.1. Packed bed reactor tests with Ni-containing DFMs at O_2-free and O_2-containing CO_2 capture conditions

Ni-based DFMs were tested with 7.5% CO_2/N_2 and with a simulated flue gas composition (7.5% CO_2/N_2 4.5% O_2, 15% H_2O balance N_2) for the CO_2 capture step. **Figure 4.2** and **Table 4.1** summarize the averaged performance (over 3 cycles) of the 10%Ni, 6.1% "Na_2O"/Al_2O_3 samples. The first sample on the left, is Al_2O_3 supported Ni^0 + adsorbent samples pre-treated at 650°C with 15% H_2/N_2. The CO_2 capture capacity is 9.55 mL under 7.5% CO_2/N_2. This high CO_2 capture capacity is attributed both to the "Na_2O"/Al_2O_3 adsorbent and Ni being fully reduced at 650°C and active for CO_2 adsorption. Its hydrogenation generated 6.74 ml of CH_4. He et al. have also reported the benefits of supporting Ni catalysts on high surface area carriers with basic sites [113]. In contrast the middle sample, also pre-reduced at 650°C, but exposed to O_2 and H_2O during the capture step, adsorbed only 2.70 ml of CO_2. However, no methane was formed due to the partial oxidation of the Ni during the capture step at 320°C. The final sample (extreme right of **Figure 4.2**) was 5%Ru, 6.1% "Na_2O"/Al_2O_3 pre-reduced at 320°C and it was included as the reference material. It adsorbed 9.43 ml of CO_2, after exposure to O_2 and steam at 320°C in the capture step. 7.11 ml of CH_4 were formed with a 75% conversion, (the difference due to CO_2 desorbed during the N_2 purge) and with no CO_2 detected after H_2 addition substantiating the role of Ru as the catalyst for DFM under simulated flue gas conditions. This latter result is to be directly compared to the Ni sample (reduced at 650°C) and exposed to O_2 and steam at 320°C (sample with 2.70 ml of CO_2 captured) with no methane production.

Reduced 10%Ni, 6.1% "Na_2O"/Al_2O_3 only produces CH_4 when the capture step is carried out under O_2-free conditions, but the moles of methane generated (276.2 mmol/kg, in **Table 4.1**) is about ½ that of 5%Ru, 6.1%"Na_2O"/Al_2O_3 DFM (614.4 mmol/kg) under similar O_2 free conditions (See **Table 4.2**). The conversion for the Ni based DFM reached only 71% (**Table 4.1**) compared to 96% for the Ru sample (See **Table 4.2**). The low carbon balance for the Ni-containing DFM (92%) can likely be attributed to CO_2 retained in the sample. It is possible that higher H_2 partial pressure may complete the reaction. Infrared studies of CO_2 adsorption on supported Ni catalysts have shown that inactive carbonate species can form on the Ni surface when Ni catalyzes a CO_2 reaction with surface oxygen species present in the carrier [114]. The formation of carbonate species on the surface of Ni DFMs can result in unreacted adsorbed CO_2 that cannot be hydrogenated at 320°C. It requires at least 800ºC for decomposition[114]. Another explanation for the incomplete carbon balance is the formation of bulk NiO on the surface of the Ni catalyst by the adsorption of CO_2 in the absence of H_2 [115,116]. According to experiments performed by Mutz et al. these oxidized species can be partially reduced at T > 400°C, but not to the original reduced state (6% NiO remains in the surface even after 20 min of H_2 exposure) and the activity of the catalyst decreased over time, likely due to sintering.

In industrial processes Ni is a preferred catalyst because it is reduced at high temperature and is never exposed to O_2. Furthermore, the process is operated close to stoichiometric conditions at high pressure [12]. We have shown that Ni is not viable under realistic flue gas conditions (O_2 present) for DFM at 320°C. We have reported that 15% H_2 is adequate to rapidly reduce the RuO_x, formed from the O_2 present in the flue gas during CO_2 capture [18] substantiating that Ru is the best catalyst for the DFM application, although reductions in its metal loading is preferred.

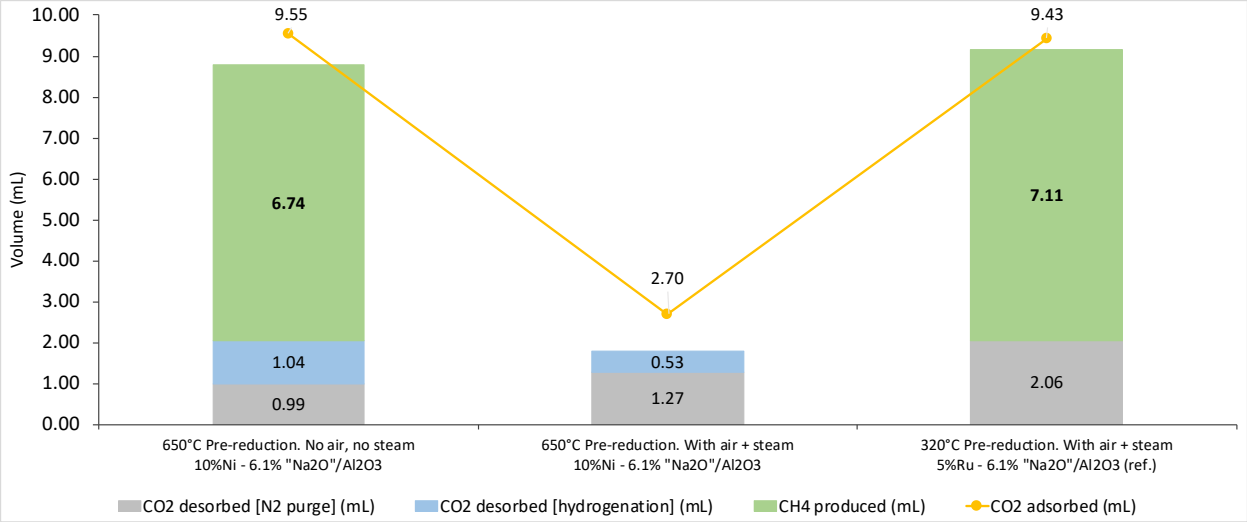

Figure 4.2. Averaged CO_2 adsorption, desorption and CH_4 produced over 3 cycles on 10% Ni, 6.1%"Na_2O"/Al_2O_3 with and without O_2 present in the CO_2 feed. 5%Ru, 6.1% "Na_2O"/Al_2O_3 included as reference. Ni samples were pre-reduced at 650°C while Ru samples at 320°C, both at 8000 h^{-1} with 15% H_2/N_2 for 2.5 h. Operation conditions: 20 min of CO_2 adsorption at 4000h^{-1} of either 7.5% CO_2/N_2 or 7.5% CO_2, 4.5% O_2, 15% H_2O balance N_2. Hydrogenation of adsorbed CO_2 at 8000 h^{-1} with 15% H_2/N_2 for 1 h. N_2 purge before and after CO_2 adsorption and methanation, 6000 h-1 for 4 min. All adsorption and hydrogenation cycles performed at 320°C and 1 atm with 1 g of sample.

Table 4.1. Summary of fixed bed reactor tests on 10% Ni, 6.1% "Na_2O"/Al_2O_3. 5%Ru, 6.1% "Na_2O"/Al_2O_3 included as reference. Operational conditions described in **Figure 4.2**. Standard error of CO_2 adsorbed, CH_4 produced, CO_2 desorbed during hydrogenation and during N_2 purge in parenthesis.

Row	Sample	Pre-reduction Temp (°C)	Air + Steam?	CO_2 adsorbed (mL)	CH_4 produced (mL)	CO_2 desorbed [hydrogenation] (mL)	CO_2 desorbed [N_2 purge] (mL)	mmol CO_2/kg-DFM	mmol CH_4/kg-DFM	Carbon balance (%)	Conv (%)
1	10%Ni, 6.1%"Na_2O"/Al_2O_3	650	No	9.55 (±0.1)	6.74 (±0.05)	1.04 (±0.2)	0.99 (±0.2)	398.2	276.2	92%	71%
2		650	Yes	2.70 (±0.1)	0	0.53 (±0.04)	1.27 (±0.1)	112.6	0	67%	0%
3	5%Ru, 6.1% "Na_2O"/Al_2O_3	320	Yes	9.43 (±0.2)	7.11 (±0.1)	0	2.06 (±0.01)	393.5	291.1	97%	75%

4.2.2. Oxidation and reducibility of 10%Ni, 6.1% "Na_2O"/Al_2O_3 samples

To better understand the oxidation and reducibility of the Ni-containing samples we studied the thermogravimetric profile of 10%Ni/Al_2O_3 when exposed to 4.5% O_2/N_2 (at 320°C) which is the typical oxygen concentration in flue gas from natural gas combustion. The exposure time was 20 min, followed by a 10 min N_2 purge (to avoid dangerous O_2 and H_2 mixture in the thermogravimetric chamber). 15% H_2/N_2 was introduced to simulate the packed bed plug flow reactor conditions previously presented. **Figure 4.3** presents the thermogravimetric profile of 10%Ni/Al_2O_3 where the reduced (at 650°C) sample is oxidized at 320°C when exposed to 4.5% O_2/N_2. Upon the introduction of hydrogen, it is not completely reduced as evidenced by the residual weight in the profile, after 6h of 15% H_2/N_2 exposure at 320°C. This is consistent with the packed bed reactor test results (presented in previous section 4.2.1) that show no methane being

formed when the Ni-containing samples are exposed to O_2 as the Ni atoms cannot be rapidly reduced to an active metallic state under hydrogen exposure at 320°C. This has been previously reported in the literature [116].

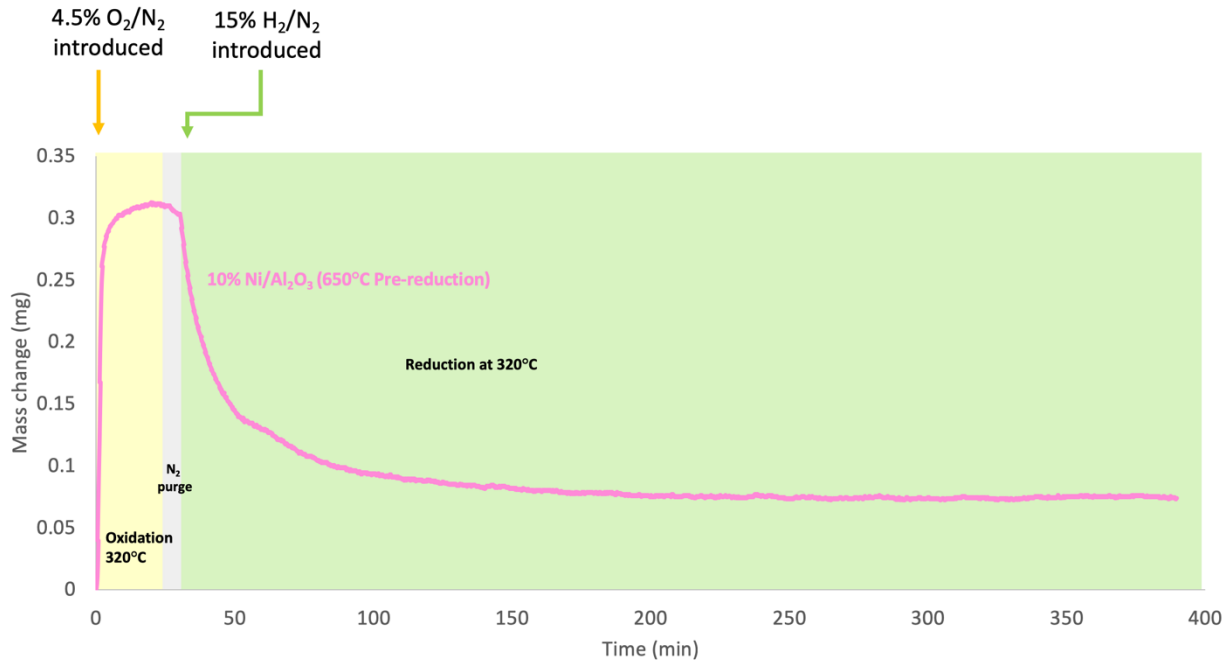

Figure 4.3. Oxidation (4.5% O_2/N_2 exposure) and reducibility (upon exposure to 15% H_2/N_2) of 10%Ni/Al_2O_3.Thermogravimetric profiles at 320°C and 1 atm. Sample initially pre-reduced with 15% H_2/N_2 at 650°C for 6h.

4.3. Influence of catalytic metals: Ru and Rh supported on 6.1% "Na_2O"/Al_2O_3.

4.3.1. Fixed bed reactor tests (in Quantachrome) as a preliminary screening tool to quantify the methanation of the adsorbed CO_2 on Ru and Rh containing DFMs.

The Ruthenium and Rhodium-based DFMs, were tested for 3 cycles of CO_2 adsorption and hydrogenation. The loading of 5%Ru and 0.5%Rh were chosen to compare similarly priced catalysts (Rh price was ~ 10x the price of Ru at the time of the study). **Figure 4.4** presents the averaged CH_4 signals. A fast and sharp methane peak is observed for the 5%Ru, 6.1% "Na_2O"/Al_2O_3. CH_4 detection occurs upon hydrogen exposure and all adsorbed CO_2 is methanated within 25 min. In contrast the 0.5% Rh, 6.1% "Na_2O" DFM sample shows a broad methane signal with reaction proceeding for an additional 10 minutes compared to the Ru DFM. This demonstrates that the Ru DFMs have a faster rate of methanation than similarly priced Rh DMFs. The amount of adsorbed CO_2 is similar for both 5%Ru and 0.5%Rh samples (1.56 and 1.5 mL respectively) but the Ru DFM converts ~100% to methane (1.50 mL of CH_4) while the Rh DFM converts only 69% of the adsorbed CO_2 to CH_4 (1.03 mL).

Table 4.2 presents a summary of the CO_2 capture and methanation capacity (both expressed in mmol /kg of DFM) for the Ru and Rh supported on 6.1% "Na_2O"/Al_2O_3 DFMs. 0.5%Rh DFM showed a similar carbon capture capacity as 5%Ru but the methanation activity was poor with less CH_4 produced per kg of material (421.9 mmol of CH_4/kg vs. 614.4 mmol of CH_4/kg).

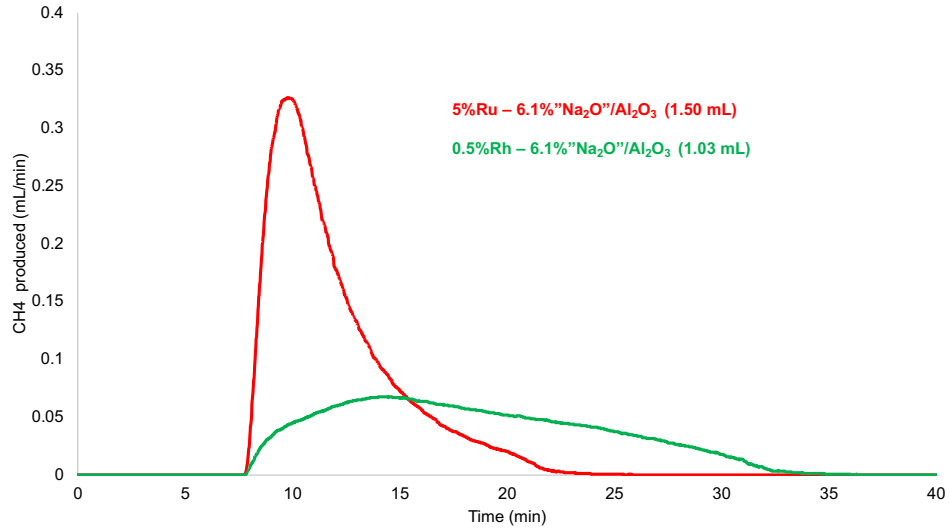

Figure 4.4. Averaged methane signal during hydrogenation step (SATP: 30 ml/min, 10% H_2/N_2 at 320°C and 1 atm) for the 5%Ru and 0.5%Rh with 6.1% "Na_2O" based DFMs

Table 4.2. Average methanation capacity of the adsorbed CO_2 on Ru and Rh DFMs supported on 6.1% "Na_2O"/Al_2O_3. CO_2 adsorption for 30 min using SATP: 30 ml/min of 10%CO_2/N_2 at 320°C. Hydrogenation of adsorbed CO_2 with SATP: 30 ml/min, 10% H_2/N_2 for 1h at 320°C. Standard error of CO_2 adsorbed and CH_4 produced in parenthesis.

Row	Sample	CO_2 ads (ml)	CH_4 (ml)	CO_2 des (ml)	mmol CO_2/ kg-DFM	mmol CH_4/ kg-DFM	Conv. efficiency (%)	C. Bal. (%)
1	5%Ru, 6.1% "Na_2O"/Al_2O_3	1.56 (±0.07)	1.50 (±0.01)	0	650.7	614.4	96%	96%
2	0.5%Rh, 6.1% "Na_2O"/Al_2O_3	1.50 (±0.06)	1.03 (±0.02)	0	625.7	421.9	69%	69%

4.3.2. Thermal Gravimetric Analysis of Ru and Rh supported on 6.1% "Na_2O"/Al_2O_3.

Figure 4.5 reports TGA weight changes for 6.1% "Na_2O" on Al_2O_3, in combination with 5%Ru (red), or 0.5%Rh (light blue). Ru and Rh containing-samples have about the same CO_2 adsorbed/kg (~ 380) but different weight loss rates indicative of the hydrogenation rates (Ru =0.1 and Rh = 0.04). **Table 4.3** summarizes all the data. The calculated rates of hydrogenation confirm the fixed bed reactor results that Ru catalyzes the fastest hydrogenation, likely due to the availability of more catalytic sites at a higher loading. We can also confirm that for the Rh DFM all the adsorbed CO_2 is removed (as CH_4 or unreacted CO_2) upon hydrogen exposure.

The relative amount of CO_2 captured can be expressed as: 0.5%Rh ~ 5%Ru. This phenomenon can be explained by the known promoting effect alkaline metal oxides have on methanation activity [117,118] as well as the enhanced adsorption (multiple CO adsorbed per Rh sites may also apply to CO_2 adsorption) of highly dispersed Rh samples with metal loadings lower than 1% by weight [119]. We have also corroborated these findings with H_2 chemisorption data obtained at room temperature (See **Table 4.8**).

All samples were pre-reduced at 320°C for 6 h with 13.26% H_2/N_2. These pretreatment conditions are adequate to reduce Ru and Rh but not for DFMs with NiO since it is only reduced at higher temperatures (>500°C)[84–86]. The 320°C represents the temperature all catalytic metals will experience in repeated cycles during DFM operations. In conclusion, Ru is the preferred catalyst for its price, fast methanation kinetics and its unique redox chemistry that allows it to be rapidly reduced upon hydrogen exposure after being exposed to O_2-containing simulated flue gas during the CO_2 capture step. Rhodium did not present any advantage over Ru and its high price makes it an unattractive candidate in a real industrial application.

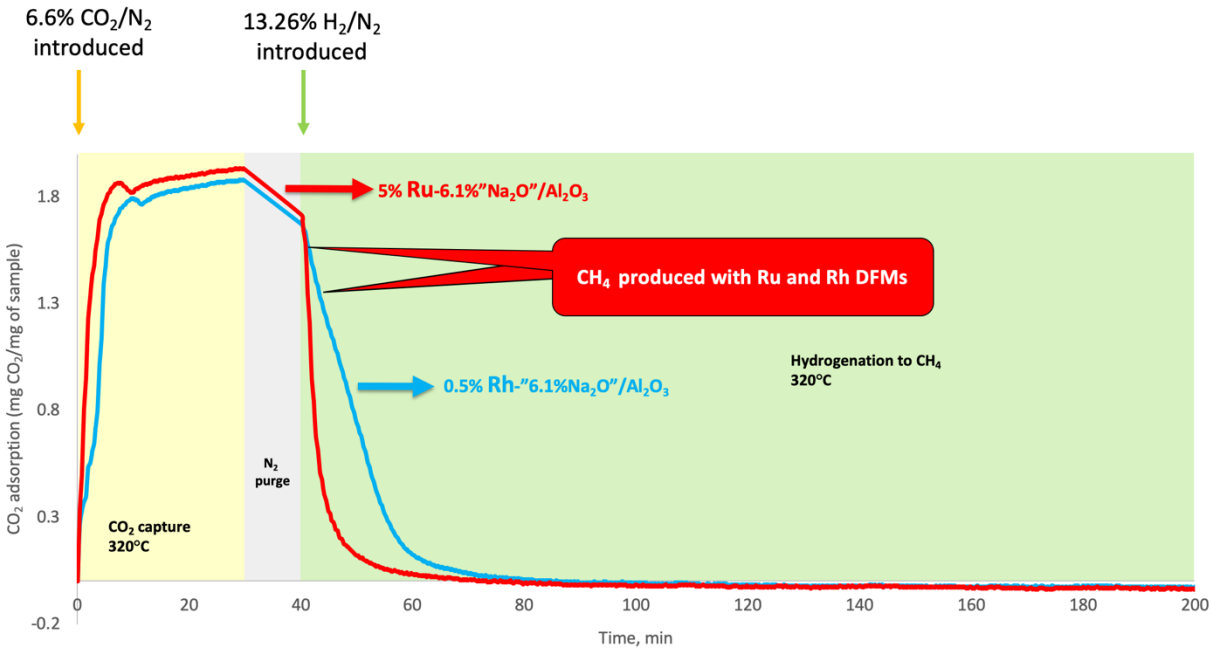

Figure 4.5. Different catalysts (5%Ru-red and 0.5%Rh-blue) co dispersed with 6.1% "Na_2O"/Al_2O_3. CO_2 capture (6.6% CO_2/N_2 exposure) and hydrogenation of adsorbed CO_2 (upon exposure to 13.26% H_2/N_2) thermogravimetric profiles at 320°C and 1 atm.

Table 4.3. Thermogravimetric analysis data for Ru and Rh catalytic metals used for DFMs supported on 6.1% "Na_2O"/Al_2O_3. All samples pre-reduced in situ at 320°C with 13.26% H_2/N_2 for 6 h.

Row	Sample	CO_2 ads (mmol CO_2/ kg sample)	Rate of hydrogenation (mg/min)	Relative rate of hydrogenation	Time to complete hydrogenation (min)
1	5%Ru, 6.1% "Na_2O"/Al_2O_3	381.4	-0.1031	2.4	36
2	0.5%Rh, 6.1% "Na_2O"/Al_2O_3	382.8	-0.0434	1	48

4.4. Influence of different alkaline adsorbents: "Na_2O", CaO, K_2O and MgO with Ru supported on Al_2O_3.

4.4.1. Fixed bed reactor tests (in Quantachrome) as a preliminary screening tool to quantify the methanation of the adsorbed CO_2 on Ru and various adsorbents (Na_2O, CaO, K_2O and MgO) supported on Al_2O_3.

We have chosen 5%Ru as our standard catalyst, based on the data presented in section 4.3. It was therefore used to test different adsorbents in DFM, the results of which are shown in **Figure 4.6**. The methane profile is similar for all samples with a sharp and rapid peak observed. Based on the amount of CO_2 adsorbed (**Table 4.4**) the best adsorbents were Al_2O_3 dispersed "Na_2O" and CaO followed by "K_2O" and MgO. The carbon capture capacity of the calcium oxide system is higher than that of sodium-based adsorbents, but the same amount of methane was generated for both DFMs, so we can only conclude that both adsorbents perform similarly under the studied conditions. **Table 4.4** presents a summary of the data generated for the Al_2O_3 supported DFMs with Ru/adsorbent variations. For all samples, ~ 91% of adsorbed CO_2 was converted to methane (with a carbon balance ~100%) with CaO and "Na_2O" showing similar methanation performance.

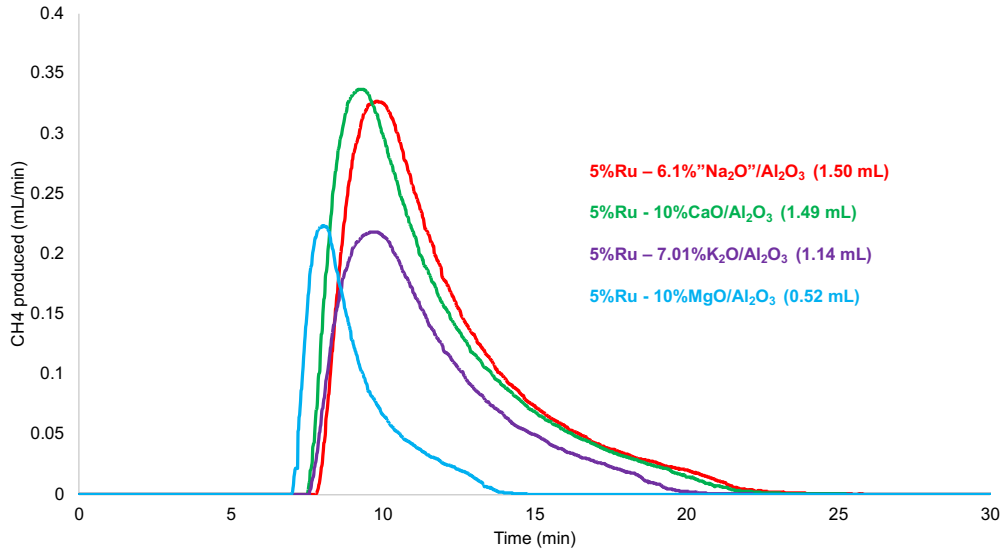

Figure 4.6. Averaged methane signal during hydrogenation step (SATP: 30 ml/min, 10% H_2/N_2 at 320°C and 1 atm) for 5%Ru on different adsorbents (10%CaO/Al_2O_3 – green , 6.1% "Na_2O"/Al_2O_3–red , 7.01% "K_2O"/Al_2O_3 – purple and 10%MgO/Al_2O_3 – light blue) DFMs.

Table 4.4. Average methanation capacity of the adsorbed CO_2 on different Dual Function Materials supported on Al_2O_3. Standard error of CO_2 adsorbed and CH_4 produced in parenthesis.

Row	Sample	CO_2 ads (ml)	CH_4 (ml)	CO_2 des (ml)	mmol CO_2/ kg-DFM	mmol CH_4/ kg-DFM	Conv. efficiency (%)	C. Bal. (%)
1	5%Ru, 6.1% "Na_2O"/Al_2O_3	1.56 (±0.07)	1.50 (±0.01)	0	650.7	614.4	96%	96%
2	5%Ru, 7.01% "K_2O"/Al_2O_3	1.19 (±0.09)	1.14 (±0.03)	0	496.4	466.9	96%	96%
3	5%Ru, 10% CaO/Al_2O_3	1.63 (±0.05)	1.49 (±0.02)	0	681.5	610.3	91%	91%
4	5%Ru, 10% MgO/Al_2O_3	0.57 (±0.05)	0.52 (±0.05)	0	237.8	213.0	91%	91%

4.4.2. Thermal Gravimetric Analysis of Ru and various adsorbents (Na_2O, CaO, K_2O and MgO) supported on Al_2O_3.

Figure 4.7 presents TGA data and **Table 4.5** presents a summary comparing different alkaline adsorbents in combination with 5%Ru supported on Al_2O_3. The adsorbent with the highest CO_2 capture capacity is 10%CaO with 425.2 mmol of CO_2/kg of DFM, however, its complete hydrogenation rate is much slower (335 min) than the Ru, "Na_2O" (36 min) DFM. "K_2O" also provides a reasonably high CO_2 capacity but its hydrogenation rate is lower (-0.086 mg/min) compared to the superior Ru, "Na_2O" DFM (-0.103 mg/min). MgO is clearly the most inferior candidate and thus is not considered a viable adsorbent.

Fast hydrogenation can be attributed to weakly chemisorbed CO_2 on CaO (CO_2-CaO) that can be easily spilled over to Ru sites to be converted to CH_4 while the slow hydrogenation can be attributed to the formation of more strongly bound CO_2-CaO [16]. Both "Na_2O" and "K_2O" adsorbents are very similar in behavior, however, "Na_2O" has a slightly better CO_2 adsorption capacity and better kinetics for hydrogenation, making it the preferred material. Infrared studies on CO_2 adsorption on "Na_2O"/Al_2O_3 have shown that doping Al_2O_3 with Na promotes the formation of ionic Al-O^- sites allowing more hydroxyl sites to be accessed for CO_2 adsorption with "Na_2O"/Al_2O_3 sorbents forming reversible bidentate and polydentate carbonates [53,54]. On the other hand, MgO showed the least CO_2 adsorption capacity with only 0.1540 mol of CO_2/kg of sample. Infrared studies have shown that MgO/Al_2O_3 is a more suitable adsorbent at lower temperatures (<150°C) since the major CO_2-MgO/Al_2O_3 bonds (bicarbonate and bidentate carbonates) are decomposed at temperatures as low as 300°C and only the unidentate carbonate sites remain active at temperatures higher than 300°C [120].

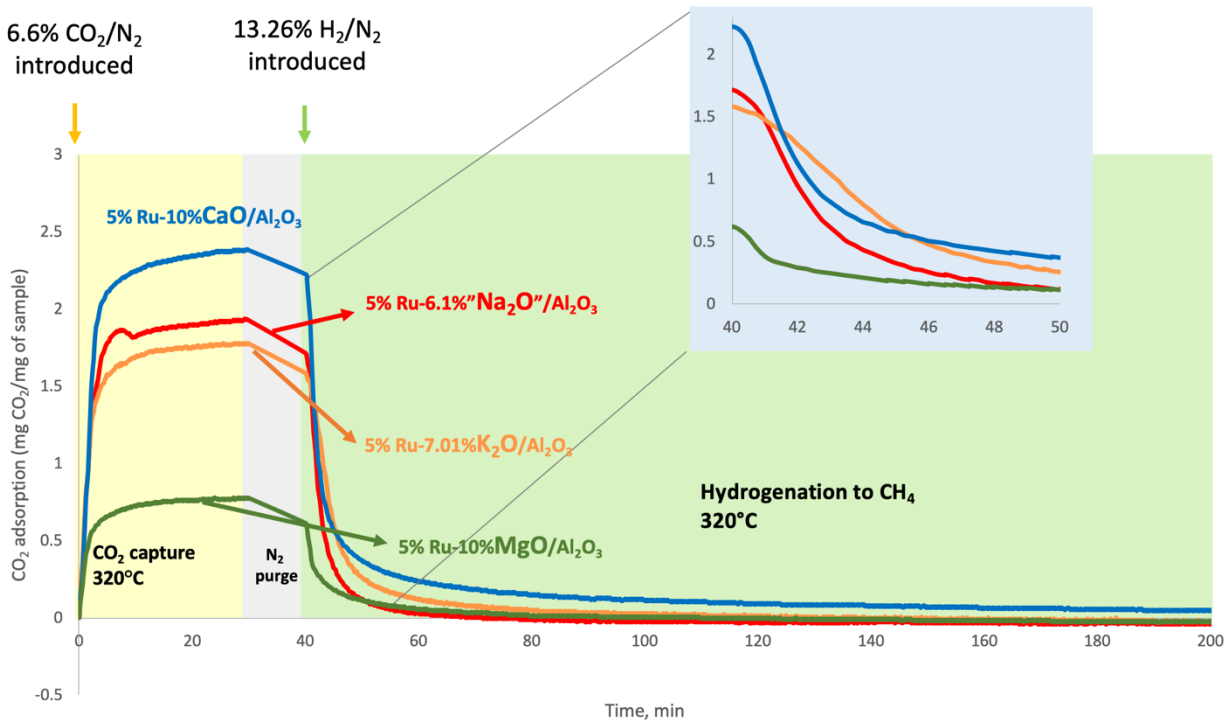

Figure 4.7. 5%Ru in combination with various adsorbents (10%CaO/Al_2O_3 – blue, 6.1% "Na_2O"/Al_2O_3 – red, 7.01% "K_2O"/Al_2O_3 – orange and 10%MgO/Al_2O_3 – green) DFMs. Thermogravimetric profiles at 320°C and 1 atm.

Table 4.5. Summary of thermogravimetric profiles of alkaline adsorbents with 5% Ru supported on Al_2O_3.

Row	Sample	CO_2 ads (mmol CO_2/ kg sample)	Rate of hydrogenation (mg/min)	Relative rate of hydrogenation	Time to complete hydrogenation (min)
1	5%Ru, 6.1% "Na_2O"/Al_2O_3	381.4	-0.1031	2.74	36
2	5%Ru, 7.01% "K_2O"/Al_2O_3	357.7	-0.0856	2.28	100
3	5%Ru, 10% CaO/Al_2O_3	425.2	-0.1300	3.48	335
4	5%Ru, 10% MgO/Al_2O_3	154	-0.0376	1	74

4.5. Influence of carriers: 5%Ru, 6.1% "Na_2O" DFM supported on Al_2O_3, CeO_2 (HSA and LSA), CZO, Na Zeolite X (Na-Z-X), H-Mordenite Zeolite (H-M-Z), SiC, SiO_2, and ZrO_2-Y.

Alternative candidate carrier materials (other than Al_2O_3) for the DFM application have also been studied. Materials such as CeO_2 (HSA: high surface area and LSA: low surface area), CeO_2/ZrO_2 (CZO), Na-Zeolite-X (Na-X-Z), H-Mordenite Zeolite (H-M-Z), SiC, SiO_2 and zirconium oxide-yttria stabilized (ZrO_2-Y) were investigated as possible alternatives to alumina as a DFM carrier. Detailed results can be found in **Figure 4.8**, **Figure 4.9**, **Table 4.6** and **Table 4.7**. Even though CeO_2 and Ceria-Zirconia (CZO) carriers show promise they do not promote the rapid conversion of the adsorbed CO_2 to CH_4 when exposed to hydrogen. They also face the disadvantage that the CeO_2 component (Ce^{+4}) can be reduced to Ce_2O_3 (Ce^{+3}) [121,122] which is an undesirable hydrogen consuming reaction.

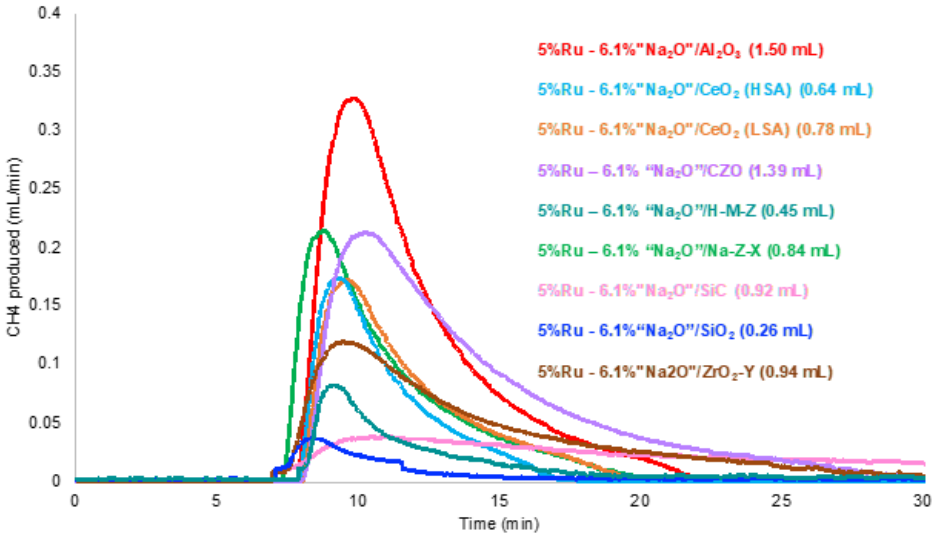

Figure 4.8. CH_4 signal during hydrogenation step for 5%Ru, 6.1% "Na_2O" supported on different carriers (Al_2O_3, CeO_2 (HAS and LSA), CZO, Na-X-Z, H-M-Z, SiC, SiO_2 and ZrO_2-Y.

Table 4.6. Average methanation capacity of the adsorbed CO_2 on 5%Ru, 6.1% "Na_2O" DFMs supported on different carriers.

Row	Sample	CO_2 ads (mL)	CH_4 (mL)	CO_2 des (mL)	CO_2/ kg-DFM	CH_4/ kg-DFM	Conv. efficiency (%)	C balance (%)
1	5%Ru-6.1%"Na_2O"/Al_2O_3 (ref.)	1.56	1.5	0	0.65	0.61	96%	96%
2	5%Ru-6.1%"Na_2O"/CeO_2 (LSA)	0.88	0.78	0	0.37	0.32	89%	89%
3	5%Ru-6.1%"Na_2O"/CeO_2 (HSA)	1.37	0.64	0	0.57	0.26	47%	47%
4	5%Ru-6.1%"Na_2O"/CZO	1.4	1.39	0.02	0.58	0.57	99%	100%
5	5%Ru-6.1%"Na_2O"/H-M-Z	1.26	0.45	0.36	0.53	0.18	36%	64%
6	5%Ru-6.1%"Na_2O"/Na-Z-X	1.65	0.84	0	0.69	0.34	51%	51%
7	5%Ru-6.1%"Na_2O"/SiC	1.41	0.92	0.46	0.59	0.38	65%	98%
8	5%Ru-6.1%"Na_2O"/SiO_2	0.57	0.26	0.04	0.24	0.11	45%	52%
9	5%Ru-6.1%"Na_2O"/ZrO_2-Y	1.04	0.94	0.08	0.43	0.39	90%	98%

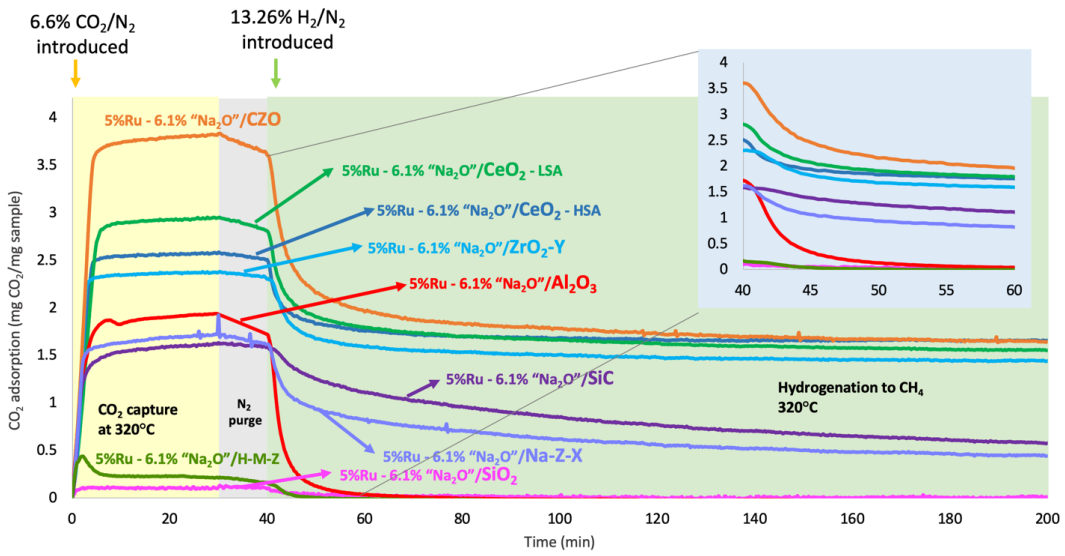

Figure 4.9. Thermogravimetric profiles for CO_2 capture capacity and hydrogenation rates for 5%Ru, 6.1%"Na_2O" impregnated on different carriers: Al_2O_3, CeO_2 (HSA and LSA), CZO, Na Zeolite X (Na-Z-X), H-Mordenite Zeolite (H-M-Z), SiC, SiO_2, and ZrO_2-Y.

Table 4.7. Summary of thermogravimetric profiles of 5%Ru, 6.1% "Na_2O" supported on different carriers

Row	Sample	CO_2 ads (mol CO_2/ kg sample)	Rate of hydrogenation (mg/min)	Relative rate of hydrogenation	Time to complete hydrogenation (min)
1	5%Ru, 6.1% "Na_2O"/Al_2O3 (ref.)	0.3814	-0.1031	54.26	36
2	5%Ru, 6.1% "Na_2O"/CeO_2-HSA	0.4980	-0.0196	10.32	indef.
3	5%Ru, 6.1% "Na_2O"/CeO_2-LSA	0.6044	-0.0404	21.26	indef.
4	5%Ru, 6.1% "Na_2O"/CZO	0.7691	-0.0421	22.16	indef.
5	5%Ru, 6.1% "Na_2O"/H-M-Z	0.0425	-0.0066	3.47	10
6	5%Ru, 6.1% "Na_2O"/Na-Z-X	0.3058	-0.0173	9.11	indef.
7	5%Ru, 6.1% "Na_2O"/SiC	0.3305	-0.0072	3.79	indef.
8	5%Ru, 6.1% "Na_2O"/SiO_2	0.0195	-0.0019	1	50
9	5%Ru, 6.1% "Na_2O"/ZrO_2-Y	0.4940	-0.0182	9.58	indef.

4.6. Characterization

The fresh DFM samples and the pristine carriers were characterized by BET, the results can be found in **Table 4.9**. The 5%Ru and 0.5%Rh impregnated on 6.1% "Na_2O"/Al_2O_3 samples were also characterized via H_2 chemisorption at room temperature and the results presented in **Table 4.8** that show that the 0.5%Rh containing sample has a dispersion of 149.2% with an average crystallite size of 0.246 nm which are significantly smaller than the 5%Ru containing samples with a dispersion of 3.9% and an average crystallite size of 13.9 nm [18]. This is in accordance to Drault et al. reporting a highly dispersed Rh catalyst with a stoichiometry of H atom adsorption/metal atom higher than 1 [106].

Table 4.8. Ru and Rh dispersion and average crystallite size derived from H_2 chemisorption at room temperature (25°C) for fresh DFM samples. *Obtained from Wang, et al. [18].

Row	Sample	Metal dispersion (%)	Average crystallite size (nm)
1	5%Ru, 6.1% "Na_2O"/Al_2O_3	3.9%*	13.9*
2	0.5%Rh, 6.1% "Na_2O"/Al_2O_3	149.2%	0.246

Table 4.9. BET surface area (m^2/g) of fresh DFM compositions and pristine carriers.

Row	Sample	SSA (m^2/g)
1	Al_2O_3	165
2	CeO_2 (LSA)	44
3	CeO_2 (HSA)	112
4	CZO	48
5	H-M-Z	335
6	Na-Z-X	376
7	SiC	2
8	SiO_2	53
9	ZrO_2-Y	11
10	5%Ru, 6.1%"Na_2O"/Al_2O_3	95
11	0.5%Rh, 6.1%"Na2O"/Al_2O_3	101
12	10%Ni, 6.1%"Na_2O"/Al_2O_3	92
13	5%Ru, 7.01%"K_2O"/Al_2O_3	95
14	5%Ru, 10%CaO/Al_2O_3	71
15	5%Ru, 10%MgO/Al_2O_3	105
16	5%Ru, 6.1%"Na_2O"/CeO_2 (LSA)	25
17	5%Ru, 6.1%"Na_2O"/CeO_2 (HSA)	47
18	5%Ru, 6.1%"Na_2O"/CZO	29
19	5%Ru, 6.1%"Na_2O"/H-M-Z	73
20	5%Ru, 6.1%"Na_2O"/Na-Z-X	125
21	5%Ru, 6.1%"Na_2O"/SiC	5
22	5%Ru, 6.1%"Na_2O"/SiO_2	43
23	5%Ru, 6.1%"Na_2O"/ZrO_2-Y	5

Chapter 5: Precious metal/Ni combinations as viable DFM catalysts in O_2-containing flue gas due to enhanced nickel oxide reducibility

The results presented in this chapter have been published in M.A. Arellano-Treviño, N. Kanani, C.W. Jeong-Potter, R.J. Farrauto, Bimetallic catalysts for CO_2 capture and hydrogenation at simulated flue gas conditions, Chem. Eng. J. 375 (2019) 121953.

In the previous chapter we demonstrated that Ni DFMs oxidize during O_2-containing CO_2 capture conditions and are not able to reduce to catalytically active Ni^0 species when exposed to hydrogen at 320°C. In this chapter we report that small amounts of precious metal (≤ 1% Pt, Pd or Ru) enhance the reduction and activation of Ni-containing DFMs towards methanation even after O_2 exposure in a flue gas. This was corroborated with thermal gravimetric analysis (TGA). In this study we attempt to replace some of the Ru in the DFM with less expensive Ni and demonstrate the advantages and disadvantages of this replacement. The PGM-doped Ni catalysts were tested at simulated flue gas conditions (O_2 and H_2O present) for CO_2 capture in a packed bed reactor.

5.1. Thermal Gravimetric Analysis: Effect of Platinum Group Metal (PGM) doping on NiO_X redox chemistry

TGA tests were conducted to observe the reduction behavior of the PGM-doped DFM at 320°C compared to 10%Ni/Al_2O_3 reference sample (green). The alkaline adsorbent was excluded to clearly observe the reduction of NiO promoted by PGMs. Removing the adsorbent provides a clearer depiction of the reduction behavior of the Ni DFMs promoted by the PGMs [53,54].

Samples of 1%Pt/Al_2O_3 (dotted red) and 1%Ru/Al_2O_3 (dotted blue) were also examined for a baseline comparison. **Figure 5.1** presents the results.

The 10% Ni/Al_2O_3 (equivalent to 12.4%NiO/Al_2O_3) sample shows a small mass loss during the 5 hours of reduction at 320°C, equivalent to about 8% reduction. There is, however, rapid and significant mass loss observed in the 1%Pt, 10%Ni/Al_2O_3 (red) and 1%Ru, 10%Ni/Al_2O_3 (blue) DFM samples. The mass loss observed for the 1%Pt, 10%Ni/Al_2O_3 and 1%Ru, 10%Ni/Al_2O_3 samples include the reduction of PtO_x and RuO_x, which can be seen in the mass loss profiles of 1%Pt/Al_2O_3 (dotted red) and 1%Ru/Al_2O_3 (dotted blue), respectively; however, the additional and much more significant mass loss is attributed to reduction of NiO_x to active metallic Ni. This is clear evidence that the reduction of NiO_x is enhanced by the presence of PGMs such as Pt or Ru. In fact, the mass loss seen for the 1%Pt, 10%Ni/Al_2O_3 sample is equivalent the full reduction of the PtO_x species and 50.3% reduction of the NiO_x species, which explains why this bimetallic pair produced methane in the packed powder reactor (see section 5.2.2.) while Pt alone did not [21]. The mass loss seen for the 1%Ru, 10%Ni/Al_2O_3 sample is equivalent to the full reduction of the RuO_x species and 70.3% reduction of the NiO_x species present in the fresh sample, again explaining the enhanced adsorption and conversion activity of this DFM as will be discussed in the following section.

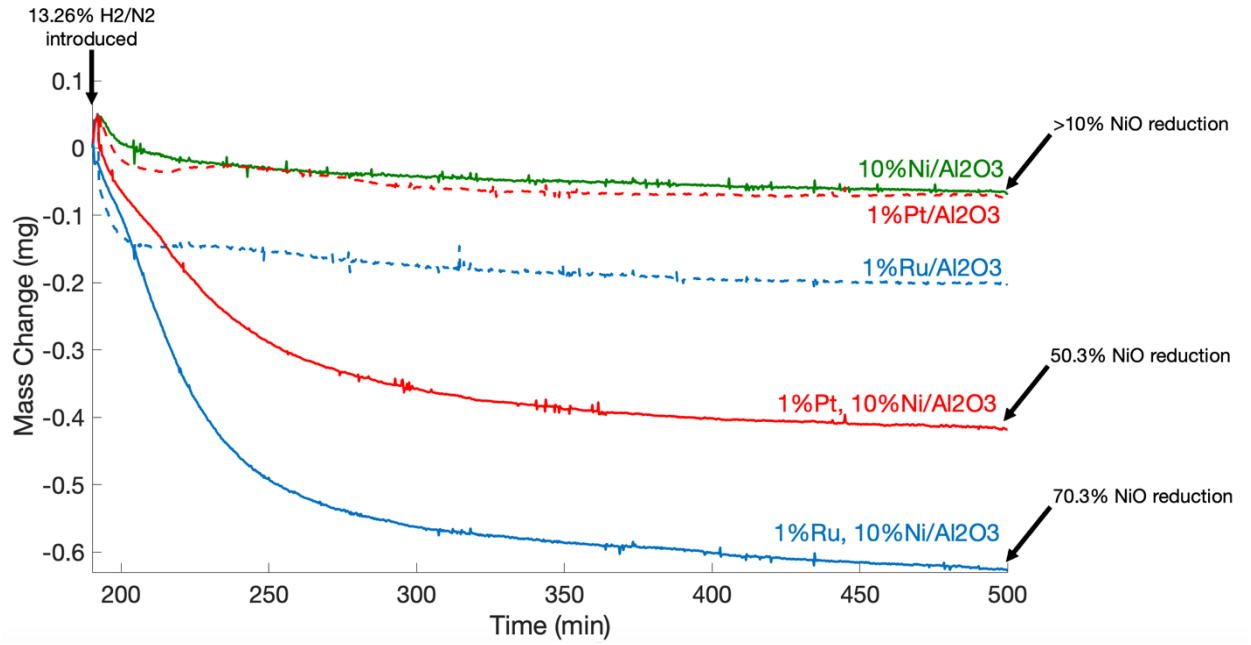

Figure 5.1. Thermal gravimetric analysis results for 30.0 mg samples of 10%Ni/Al_2O_3 (green), 1%Pt/Al_2O_3 (red), 1%Ru/Al_2O_3 (blue), 1%Pt, 10%Ni/Al_2O_3 (red), 1%Ru, 10%Ni/Al_2O_3 (blue) reduced in 13.26% H_2/N_2 for 5 hours at 320°C. It must be pointed out that supported Ni is present initially as the oxide and partially reduced during the reduction. Figure generated by Chae Jeong-Potter.

5.2. Packed bed reactor tests with simulated flue gas conditions

5.2.1. PGM (Pt, Pd or Ru) doping (≤1%) to 10%Ni, 6.1% "Na_2O" /Al_2O_3 DFM

Figure 5.2A presents the detail of the 3 cycles of CO_2 adsorption (with O_2 and H_2O present) and CH_4 produced along with CO_2 desorbed (CO_2 desorbed = CO_2 desorbed from N_2 purge + CO_2 desorbed during hydrogenation). In all results presented in section 5.2 and 5.3, the amount of CO_2 desorbed during the hydrogenation represented less than 5% of the total with most of the

contribution coming from the CO_2 desorbed during the N_2 purge. This is an experimental artifact of the reactor dead volume. **Table 5.1** summarizes the detail of each cycle as well as the average and provides conversion of CO_2 to CH_4 (calculated with equation 5.1). The conversion to CH_4 is calculated based on CO_2 retained on the sample after the purge.

$$Conversion = \frac{CH_4\ produced}{CO_2\ adsorbed - CO_2\ desorbed\ during\ N_2\ purge} x100\% \quad (5.1)$$

In **Figure 5.2A** we have included some of the previous results study where it was demonstrated that 10% Ni, 6.1% "Na_2O"/Al_2O_3 adsorbs very little CO_2 at simulated flue gas conditions (average of 0.11 mmol of CO_2 adsorbed) and produces no CH_4 when exposed to hydrogen [123]. These results are included as a reference to be compared to the PGM-promoted Ni samples which highlight the impact of a small loading of PGM (like Pt and Ru) on Ni-containing DFMs. It is clear from **Figure 5.1**, that one of the benefits of doping Ni with small amounts of precious metals is the lowering of the temperature for NiO_x reduction. For the 0.1% Pt, Ni-containing DFMs, CO_2 capture (0.39 mmol of average CO_2 adsorbed) was due mainly to the "Na_2O" present, which produced 0.16 mmol of CH_4 due to the enhanced reduction promoted by Pt. It should be noted that Pt alone does not produce CH_4 [21]. At a Pt loading of 1%wt. methanation activity is furtherly enhanced due to increased reduction of Ni (0.25 mmol of average CH_4 produced) with a slightly lower average CO_2 capture capacity (0.35 mmol of CO_2/g) attributed to less "Na_2O"/Al_2O_3 sites available at the expense of higher metal loading. By far, 0.1%Ru shows the greatest promotional effect for the reduction of NiO_x with an average of 0.5 mmol of CO_2 adsorbed and 0.32 mmol of methane produced.

The conversion and carbon balances can be found in **Table 5.1**. The poor carbon balance values (for NiO_x only, Pt, Ni and 0.1%Ru, Ni) can be explained by the low rate of methane formation presented in **Figure 5.2B**. Both Pt samples show slow rates of methane formation when compared to the 0.1%Ru, Ni system that presents the sharpest peak for CH_4 generation. However, the rates of methanation are not fast enough to hydrogenate all the adsorbed CO_2 (see rates in **Figure 5.3B** for comparison) resulting in unreacted adsorbed CO_2 remaining on the surface of the DFMs.

We can conclude that for the samples presented in **Figure 5.2B**, the CO_2 on the adsorbent sites are not fully desorbed at the end of the hydrogenation step and therefore the adsorbant is not active for CO_2 capture in the subsequent cycles. Overall, the 0.1%Ru, 10%Ni, 6,1% "Na_2O"/Al_2O_3 sample has the highest average CO_2 capture capacity and methanation because Ru has the highest exothermic heat rate, enhancing CO_2 spillover (desorption) making more CO_2 adsorbent sites available for subsequent adsorption. Pt has a lower methanation and heat rate and therefore is not as effective as Ru. **Table 5.1** presents the detail of the cycles and a declining trend of CO_2 capture capacity can be appreciated for all the Pt-Ni systems and the 0.1%Ru-Ni system which corroborates this hypothesis.

In-situ infrared studies performed on the surface of Ru, "Na_2O"/Al_2O_3 DFMs [17] indicate that CO_2 adsorption occurs mainly in Al—O^-—Na^+ adsorbent sites both as bicarbonates and bidentate carbonates while catalyst sites are oxidized in the presence of O_2-containing flue gas. Upon the addition of hydrogen, the RuO_x sites are rapidly reduced to metallic Ru. The CO_2 spills over to the Ru sites to be converted to CH_4 and water via formate species in an exothermic reaction that drives the spillover of more CO_2 to catalyst sites. In the case of PGM-promoted Ni DFMs we can speculate that PtO_x and RuO_x are rapidly reduced to their metallic state and aid the reduction

of NiO_x at lower temperatures by splitting hydrogen atoms to readily reduce NiO_x [106,107]. In the case of Ru, Ni DFMs, CO_2 would spill over to both Ni and Ru sites to be converted to CH_4 and water. In the case of Pt-Ni DFMs only Ni would methanate CO_2 since Pt is not active for this reaction [21].

The activity of the 0.1%Pd, Ni sample is also included in **Table 5.1** for reference. Pd-containing samples took longer times to complete hydrogenation (~90 min) and the rate of methane formation was the slowest of all the PGM-Ni systems. In addition to generally low CH_4 production, Pt-containing DFMs showed lower hydrogenation rates (as shown in **Figure 5.2B**). Neither high nor low Pt or Pd loading samples were very encouraging and because of their high cost and lower methanation rates, no priority for this application will be given relative to the superior performance of the Ru, Ni combination.

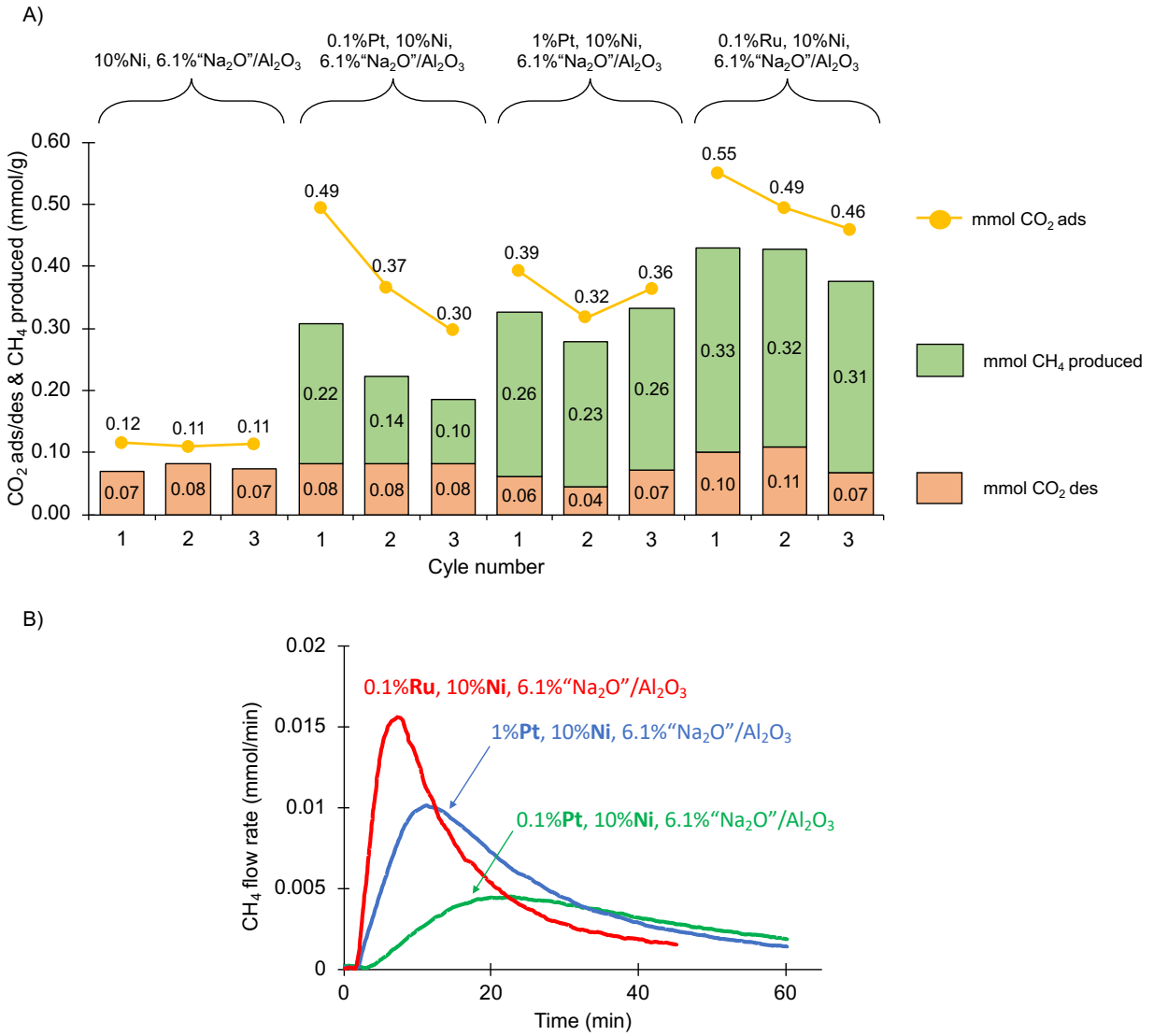

Figure 5.2. The positive influence of doping PGM (Ru and Pt) to promote 10%Ni, 6.1% "Na_2O"/Al_2O_3 for use as a DFM when exposed to simulated flue gas. A) CO_2 adsorption, desorption and CH_4 produced over 3 cycles. B) Averaged CH_4 production peaks recorded during hydrogenation step. Operation conditions presented in **Figure 3.1.**

5.2.2. Effect of Ru doped Ni catalysts in CO_2 capture capacity and methanation rate of DFM

A higher loading of Ru was furtherly studied (1%Ru, 10%Ni, 6.1% "Na_2O"/Al_2O_3) both in the presence and absence of Ni in the DFMs composition. **Figure 5.3A** presents the results over 3 cycles of CO_2 capture + hydrogenation. 1%Ru, 10%Ni, 6.1% "Na_2O"/Al_2O_3 appears to be the most promising combination having the highest CO_2 adsorption (average of 0.52 mmol of CO_2 ads) and average CH_4 production of 0.38 mmol for a hydrogenation duration of 30 mins. The 0.1%Ru, 10%Ni, 6.1% "Na_2O"/Al_2O_3 also showed satisfactory results by producing an average of 0.32 mmol of CH_4 in 45 mins.

The Ru impregnated sample 1% Ru, 6.1% "Na_2O"/Al_2O_3 showed the fastest methanation profile indicated by the sharp methane production rate (presented in **Figure 5.3B** as shown more clearly in the in insert). **Table 5.2** presents the slopes of the initial methanation rate where we confirm that the slope of the methane peak for this sample (4.4 ml/min^2) is the steepest and ~176 times faster than the slowest sample (0.1%Ru, 6.1% "Na_2O"/Al_2O_3) used as a reference rate 1. However, its performance in terms of average CO_2 adsorption (0.41 mmol of CO_2 ads) and CH_4 produced (0.31 mmol of CH_4) were lower compared to the 1%Ru-Ni system. The presence of 10% Ni with 1% Ru, showed a lower methanation rate (1.8 ml/min^2 from **Table 5.2**) with a broader peak shifted to longer times due to the lower methanation activity of Ni compared to Ru only. However, both the CO_2 adsorption and CH_4 produced were significantly higher than the Ni free system (see **Table 5.1**).

At lower Ru loadings (0.1%) the benefit of having Ni becomes even more evident. In **Figure 5.3B**, 0.1%Ru with no Ni (green) shows the lowest methanation rate (0.025 ml/min^2 from **Table 5.2**) while 0.1%Ru with 10%Ni (red) shows a 4 times higher rate of methane production (0.11 ml/min^2 from **Table 5.2**) . This is additional proof that Ni is contributing to methanation. It

is also appreciated from **Figure 5.3A** that in average, all the samples containing Ni in the Ru-Ni system adsorb more CO_2 and produce more methane under similar conditions compared to the Ni free Ru DFMs. For the 0.1%Ru-containing samples, it can be appreciated in **Table 5.1** that both samples have similar CO_2 capture capacities in cycle #1 and the 0.1%Ru, 10%Ni sample, having a better methanation and heat rate compared to the Ni-free sample was able to regenerate more CO_2 adsorbent sites after each cycle, which would explain its higher average CO_2 capture capacity and methane produced. However, for the sample with 1%Ru, 10%Ni, the CO_2 capture capacity is higher than the Ni-free sample starting with cycle #1. We hypothesize that the reason for the higher CO_2 capture capacity is likely explained by CO_2 adsorption on passivated NiO_x sites [100,124].

The 0.1%Ru, 10%Ni sample did not perform as well as 1%Ru, 10%Ni which is likely due to the low Ru loading that results in a slower rate of methanation. Nonetheless, 0.1%Ru, 10%Ni (and other Ru/Ni ratios) remains a promising alternative when considering economic cost trade-offs. With further material optimization and reactor design < 1% Ru loadings may be viable.

The Ru-containing Ni DFMs had average material balances close to or greater than 90% except for 0.1%Ru, 10%Ni at 82%. Conversion was close to or above 80% for the Ru DFMs (see **Table 5.1**). Overall, at higher Ru loadings, Ru-only samples showed a faster and sharper CH_4 formation peak. However, the Ru-Ni systems outperformed the others in terms of enhanced CO_2 adsorption (all Ni-containing samples adsorbed more CO_2) but more extensive aging (>20 cycles) is necessary to ensure stability.

It is also important to mention that in all O_2-containing CO_2 adsorption steps there was a small temperature rise (~10°C) observed in the catalyst bed in the first 5 seconds that rapidly stabilized. This temperature increase is associated with two exothermic events: adsorption of CO_2

and oxidation of metallic sites. It is suspected that oxidation of nickel is the main contributor to the temperature rise. For the 1%Ru, 10%Ni sample this exotherm was more pronounced (~80°C) as more Ni sites (from the previous hydrogenation step) were available for oxidation. This can become a more important issue as we scale up Ni-containing DFMs since it would be necessary to prevent dangerous hot spots in the packed bed associated with rapid Ni oxidation.

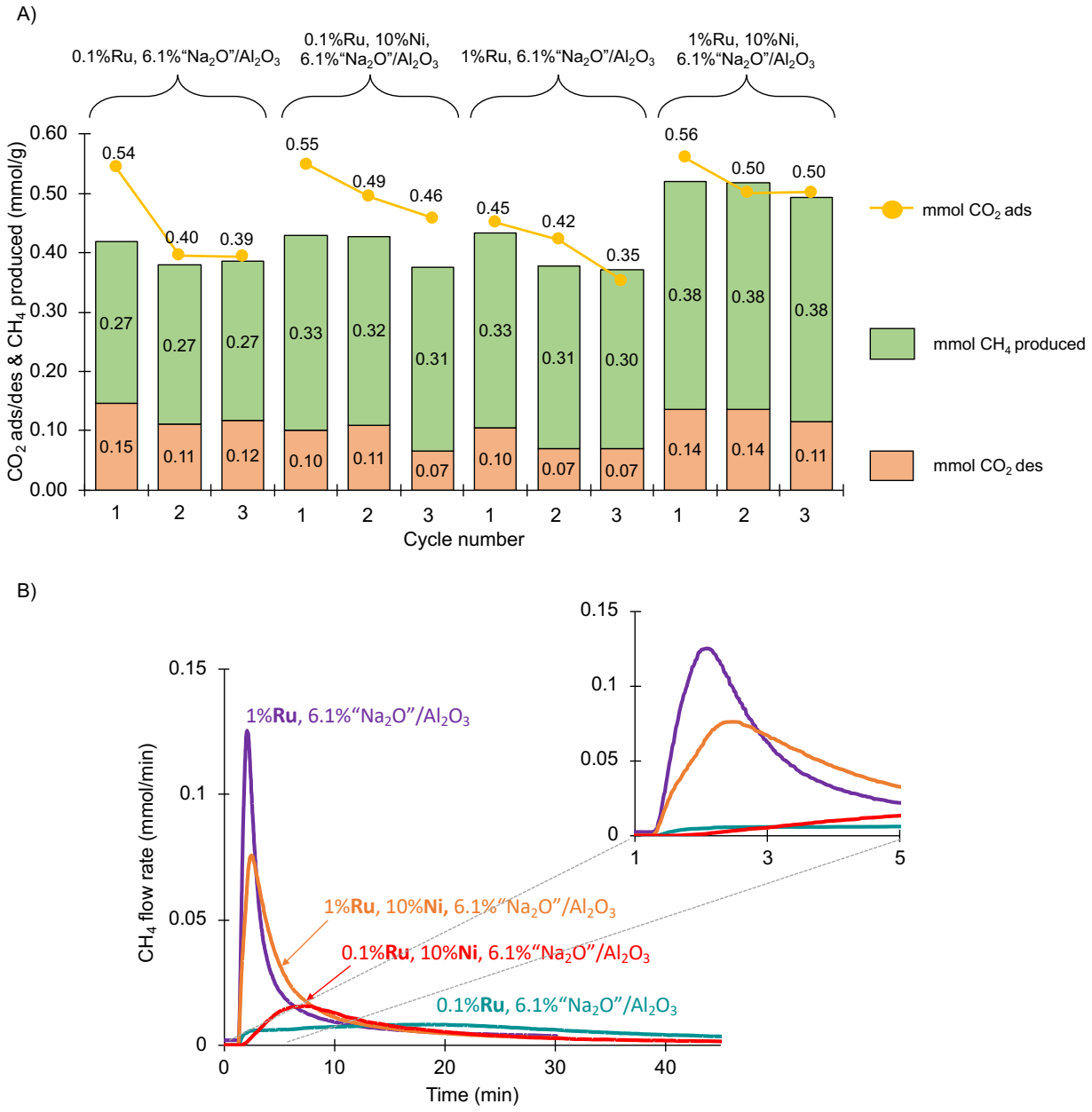

Figure 5.3. Effect of Ni on Ru-containing DFMs. A) CO_2 adsorption, desorption and CH_4 produced over 3 cycles for Ni-containing and Ni-absent DFMs with low (0.1%) and high (1%) Ru loading. B) Averaged CH_4 production rates recorded during the hydrogenation step. Same operational conditions as in **Figure 3.1.**

Table 5.1. Detail of the cycles of the packed bed reactor tests presented in **Figure 5.2** and **Figure 5.3**. Operational conditions described in **Figure 3.1.**

Sample	Pre-reduction Temp (°C)	CO_2 adsorbed (mmol/g)	CH_4 produced (mmol/g)	CO_2 desorbed [hydrogenation] (mmol/g)	CO_2 desorbed [N_2 purge] (mmol/g)	CO_2 desorbed (mmol/g)	Conv (%)	Carbon balance (%)
10%Ni, 6.1%"Na_2O"/Al_2O_3	650	0.12	0.00	0.03	0.04	0.07	0%	60%
		0.11	0.00	0.02	0.06	0.08	0%	76%
		0.11	0.00	0.02	0.05	0.07	0%	66%
Average		**0.11**	**0.00**	**0.02**	**0.05**	**0.08**	**0%**	**67%**
0.1% Pd, 10%Ni, 6.1%"Na_2O"/Al_2O_3	500	0.53	0.23	0.00	0.16	0.16	62%	74%
		0.38	0.14	0.00	0.14	0.14	58%	74%
		0.49	0.19	0.00	0.13	0.13	52%	64%
Average		**0.47**	**0.18**	**0.00**	**0.14**	**0.14**	**57%**	**71%**
0.1% Pt, 10%Ni, 6.1%"Na_2O"/Al_2O_3	500	0.49	0.22	0.00	0.08	0.08	55%	62%
		0.37	0.14	0.00	0.08	0.08	50%	61%
		0.30	0.10	0.00	0.08	0.08	48%	62%
Average		**0.39**	**0.16**	**0.00**	**0.08**	**0.08**	**52%**	**62%**
1% Pt, 10%Ni, 6.1%"Na_2O"/Al_2O_3	500	0.39	0.26	0.00	0.06	0.06	80%	83%
		0.32	0.23	0.00	0.04	0.04	86%	88%
		0.36	0.26	0.00	0.07	0.07	89%	91%
		0.34	0.26	0.00	0.06	0.06	94%	95%
Average		**0.35**	**0.25**	**0.00**	**0.06**	**0.06**	**87%**	**89%**
0.1%Ru, 10%Ni, 6.1%"Na_2O"/Al_2O_3	320	0.55	0.33	0.00	0.10	0.10	73%	78%
		0.49	0.32	0.00	0.11	0.11	82%	86%
		0.46	0.31	0.00	0.07	0.07	79%	82%
Average		**0.50**	**0.32**	**0.00**	**0.09**	**0.09**	**78%**	**82%**
0.1%Ru, 6.1%"Na_2O"/Al_2O_3	320	0.54	0.27	0.00	0.15	0.15	68%	77%
		0.40	0.27	0.00	0.11	0.11	94%	96%
		0.39	0.27	0.00	0.12	0.12	97%	98%
Average		**0.44**	**0.27**	**0.00**	**0.12**	**0.12**	**84%**	**89%**
1%Ru, 10%Ni, 6.1%"Na_2O"/Al_2O_3	320	0.56	0.38	0.07	0.06	0.14	77%	93%
		0.50	0.38	0.08	0.06	0.14	86%	104%
		0.50	0.38	0.08	0.03	0.11	81%	98%
Average		**0.52**	**0.38**	**0.08**	**0.05**	**0.13**	**81%**	**98%**
1%Ru, 6.1%"Na_2O"/Al_2O_3	320	0.45	0.33	0.05	0.06	0.10	84%	96%
		0.42	0.31	0.01	0.06	0.07	84%	90%
		0.35	0.30	0.01	0.06	0.07	101%	105%
Average		**0.41**	**0.31**	**0.02**	**0.06**	**0.08**	**89%**	**96%**

Table 5.2. Comparison of the slopes of the initial methanation rate peaks presented in **Figure 5.3B**. The slopes were calculated within the first 3 min of methanation. The relative rate is calculated by normalizing the slopes with the slowest rate stated as a reference of 1.

Sample	Initial methanation rate slope (ml/min^2)	Relative rate
0.1% Ru, 6.1% "Na_2O"/Al_2O_3	0.025	1
0.1% Ru, 10%Ni, 6.1% "Na_2O"/Al_2O_3	0.11	4
1% Ru, 10%Ni, 6.1% "Na_2O"/Al_2O_3	1.8	72
1% Ru, 6.1% "Na_2O"/Al_2O_3	4.4	176

5.3. Cyclic aging studies in O_2 and H_2O-containing simulated flue gas for the capture step using Ru doped Ni DFM

1% Ru, 10% Ni, 6.1% "Na_2O"/Al_2O_3 DFM was chosen for extended aging studies based on its good CO_2 capture capacity and CH_4 production. **Figure 5.4** shows the cyclic aging performed with 1 g of powdered sample. The results are presented as an average for every 4 cycles. The sample was aged for 20 cycles showing a stable performance. Both conversion and mass balances are close to 100% in all cycles with the performance improving slightly after the 4^{th} cycle. **Table 5.3** presents the detailed information on the aging studies.

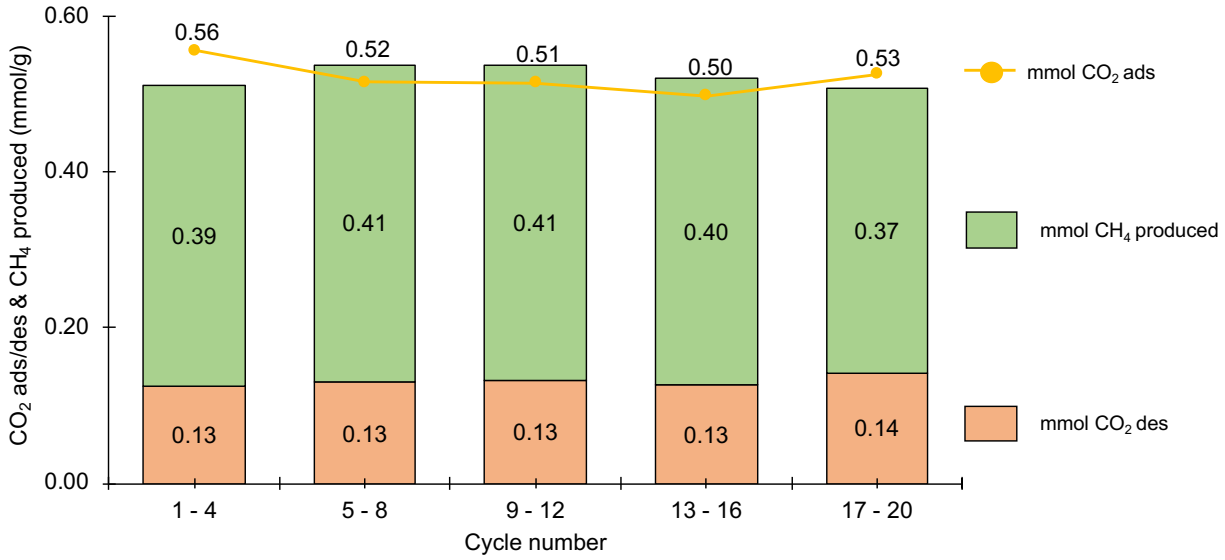

Figure 5.4. 20 cycle tests under simulated flue gas conditions on 1 g of powdered 1%Ru, 10%Ni, 6.1% "Na_2O"/Al_2O_3 DFM. Operation conditions: 20 min of CO_2 adsorption (4000 h^{-1}: 7.5%CO_2, 4.5% O_2, 15% H_2O balance N_2). Hydrogenation of adsorbed CO_2 (8000 h^{-1}: 15% H_2/N_2) for 30 min. N_2 purge (6000 h^{-1}) before and after CO_2 adsorption and methanation, for 4 min. All adsorption and hydrogenation cycles performed at 320°C and 1 atm.

We propose the following reactions during DFM process (all steps at 320°C):

1. Capture step in O_2-containing flue gas: Both Ru and Ni are partially oxidized, CO_2 adsorbs on "Na_2O"/Al_2O_3 and to a limited extent on NiO_x sites:

$$Na_2O"/Al_2O_3 + CO_2 \rightarrow CO_2 \cdots Na_2O"/Al_2O_3 \quad (5.2)$$

$$Ru/Al_2O_3 + \frac{x}{2}O_2 \rightarrow RuO_x/Al_2O_3 \quad (5.3)$$

$$Ni/Al_2O_3 + \frac{y}{2}O_2 + CO_2 \rightarrow CO_2 \cdots NiO_y/Al_2O_3 \quad (5.4)$$

2. Hydrogenation step. Reduction of Ru and Ni to their active metallic state. CO_2 spill over from "Na_2O"/Al_2O_3 to Ru and Ni for methanation.

$$RuO_x/Al_2O_3 + xH_2 \rightarrow Ru/Al_2O_3 + xH_2O \quad (5.5)$$

$$CO_2 \cdots NiO_y/Al_2O_3 + (y+4)H_2 \rightarrow Ni/Al_2O_3 + CH_4 + (y+2)H_2O \quad (5.6)$$

$$CO_2 \cdots Na_2O"/Al_2O_3 + 4H_2 \xrightarrow{Ru,Ni/Al_2O_3} Na_2O"/Al_2O_3 + CH_4 + 2H_2O \quad (5.7)$$

PGM promoted Ni-containing DFM is a promising technology for capturing and catalytically converting CO_2 to synthetic fuel in situ. We believe a scale-up of the process to 1 kg of DFM with detailed economics is worthy of pilot studies for possible future commercialization.

Table 5.3. Aging studies of 1 g of powder 1%Ru, 10%Ni, 6.1% "Na_2O"/Al_2O_3 DFM. Results averaged every 4 cycles for a total of 20 cycles. Operational conditions presented in **Figure 5.4**. Conversion calculated with equation 5.1. Standard error of CO_2 adsorbed/desorbed and CH_4 produced in parenthesis.

Cycle #	mmol CO_2 adsorbed/g	mmol CH_4 produced/g	mmol CO_2 desorbed/g	Conv (%)	Carbon balance (%)
1 - 4	0.56 ($\pm 3x10^{-2}$)	0.39 ($\pm 2x10^{-3}$)	0.13 ($\pm 2x10^{-3}$)	90	92
5 - 8	0.52 ($\pm 2x10^{-3}$)	0.41 ($\pm 1x10^{-2}$)	0.13 ($\pm 1x10^{-2}$)	106	104
9 - 12	0.51 ($\pm 1x10^{-3}$)	0.41 ($\pm 1x10^{-2}$)	0.13 ($\pm 8x10^{-3}$)	106	105
13 - 16	0.50 ($\pm 1x10^{-2}$)	0.40 ($\pm 6x10^{-3}$)	0.13 ($\pm 7x10^{-3}$)	106	105
17 - 20	0.53 ($\pm 3x10^{-3}$)	0.37 ($\pm 5x10^{-3}$)	0.14 ($\pm 2x10^{-3}$)	95	96

5.4. Characterization

5.4.1. BET and H_2 chemisorption

The fresh and aged samples were characterized by BET and H_2 chemisorption (at 100°C) and the results presented in **Table 5.4**. The BET shows that the aged DFM had a slightly higher BET surface area after the 20 cycles but most importantly no sign of carrier sintering. A change in the Ru and Ni metal sites was evident from the H_2 chemisorption of the fresh (0.03 mmol H_2/g) vs. the spent sample (0.05 mmol H_2/g) consistent with the stability of the system after 20 cycles of aging. The results are consistent with previously published performance of the 5%Ru, 6.1% "Na_2O"/Al_2O_3 system that demonstrates stable performance of the tableted DFM after 50 cycles in simulated flue gas conditions [18].

Table 5.4. BET surface area and metal dispersion together with average catalyst crystallite size derived from H_2 chemisorption at 100°C for both fresh and aged DFMs.

Sample	BET (m^2/g)	mmol H_2 adsorbed/g
1%Ru, 10%Ni, 6.1%"Na_2O"/Al_2O_3 (fresh)	86	0.03
1%Ru, 10%Ni, 6.1%"Na_2O"/Al_2O_3 (aged 20 cycles)	99	0.05

5.4.2. XRD

X-ray diffraction patterns for fresh and aged 1%Ru, 10%Ni, 6.1% "Na_2O"/Al_2O_3 DFMs are shown in **Figure 5.5**, the patterns of 10%Ni, 6.1% "Na_2O"/Al_2O_3, 1%Ru, 6.1% "Na_2O"/Al_2O_3 and γ-Al_2O_3 were included for comparison. The representative peaks at 2θ of 39.5°, 46° and 67°

associated with the carrier γ-Al_2O_3 (111), γ-Al_2O_3 (002) and γ-Al_2O_3 (022) respectively were retained for all samples.

In the fresh Ru-doped Ni DFM and 1%Ru, 6.1% "Na_2O"/Al_2O (reference) patterns, peaks located at 2θ of 27.7°, 34.7° and 53.7° are associated with RuO_2 (110), RuO_2 (011) and RuO_2 (121) respectively. RuO_2 species are formed mainly in the calcination step in air during the material preparation, it being the most stable oxidation state. Of the three identified peaks, two vanished in the aged bimetallic DFM pattern indicating only a minimal amount of RuO_2 is retained after exposure to H_2 for sufficient time. We suspect that some of the metallic Ru species are oxidized when in contact with air at room temperature.

Similarly, in the fresh Ru-doped Ni sample and 10%Ni, 6.1% "Na_2O"/Al_2O (reference) patterns, peaks located at 2θ of 37°, 42.9°, 62.4°, 74.8° and 78.8° are associated with NiO (111), NiO (002), NiO (022), NiO (113) and NiO (222), which are formed during the calcination step of the material synthesis process. Of the 5 NiO peaks identified, none were visible on the aged bimetallic sample. We hypothesize that the NiO crystals developed an (XRD invisible) amorphous pattern due to the redispersion (significant reduction in size) of the nickel sites after the extensive oxidation/reduction cycles. Also, there is evidence that some of the NiO was completely reduced to metallic Ni when exposed to hydrogen with the help of the promoting effect of Ru doping. We speculate that the broad peak shown in the aged Ru-doped Ni DFM pattern at 2θ of 44.5° corresponds to a mixture of Ru (011 at 44°) and Ni (111 at 44.7°) indicating the presence of both metallic Ru and Ni.

The decomposition of supported Na_2CO_3 on Al_2O_3 is speculated to generate 6.1%"Na_2O"/Al_2O_3. Previous imaging from STEM-EDX mapping shows a very well dispersed Na adsorbent [18] so we conclude the corresponding X-ray diffraction pattern is amorphous.

Moreover, characteristic Na_2O peaks at 2θ of 45.8° and 66.8° corresponding to Na_2O (022) and Na_2O (004) are masked by γ-Al_2O_3 (002) and γ-Al_2O_3 (022) peaks respectively. However, a peak at 2θ of 32° associated with Na_2O (002) was observed in the aged Ru-doped Ni DFM and the fresh reference materials, yet it was not identified in the fresh Ru-doped Ni DFM.

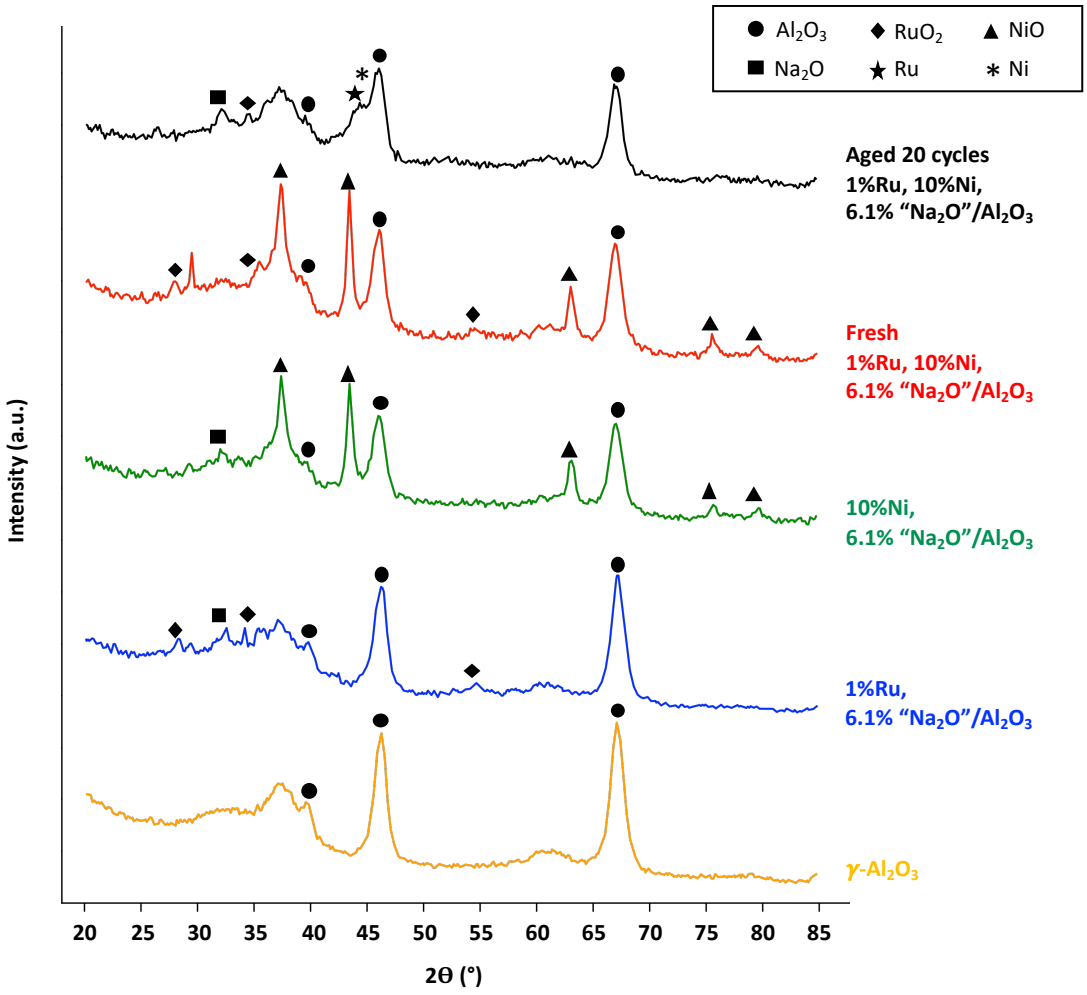

Figure 5.5. X-ray diffraction patterns of fresh (red) and aged (black) 1%Ru, 10%Ni, 6.1% "Na_2O"/Al_2O_3 samples. 10%Ni, 6.1% "Na_2O"/Al_2O_3 (green), 1%Ru, 6.1% "Na_2O"/Al_2O_3 (blue) and γ-Al_2O_3 (yellow) patterns included for comparison.

5.4.3. TEM-EDS

A detailed analysis of the microstructure and composition of both fresh and aged 1%Ru, 10%Ni, 6.1% "Na_2O"/Al_2O_3 surfaces were obtained via transmission electron microscopy (TEM). In order to differentiate the various elements present we used the scanning transmission electron microscope (STEM) energy-dispersive X-ray spectroscopy (EDS) mapping. **Figure 5.6A** presents the image taken from the fresh sample with the mapping of the Ru, Ni and Na species. We can see that the Ru-rich cluster (encircled in light blue) and the Ni-rich clusters (encircled in pink) are of similar size of about 58 nm and 53 nm respectively.

In **Figure 5.6B** we can see the aged sample's surface with its respective EDS mapping. The Ni-rich areas appear to be more uniformly scattered throughout the sample with smaller clusters (when compared to their fresh counterpart) encircled in pink. Ru-rich clusters are similarly smaller (encircled in light blue). Both Ru and Ni clusters in the aged sample are of similar size of approximately 19 nm. The Ru and Ni cluster size decrease trend corroborates the H_2 chemisorption results presented in **Table 5.4** that show an increase in H_2 uptake that evidences some redispersion of the Ru and Ni sites after 20 oxidation/reduction cycles.

In neither the fresh nor aged sample we could see evidence of metal alloy formation. All other elemental components of the sample (Na, Al, O) show a very well dispersed EDS mapping for both fresh and aged samples.

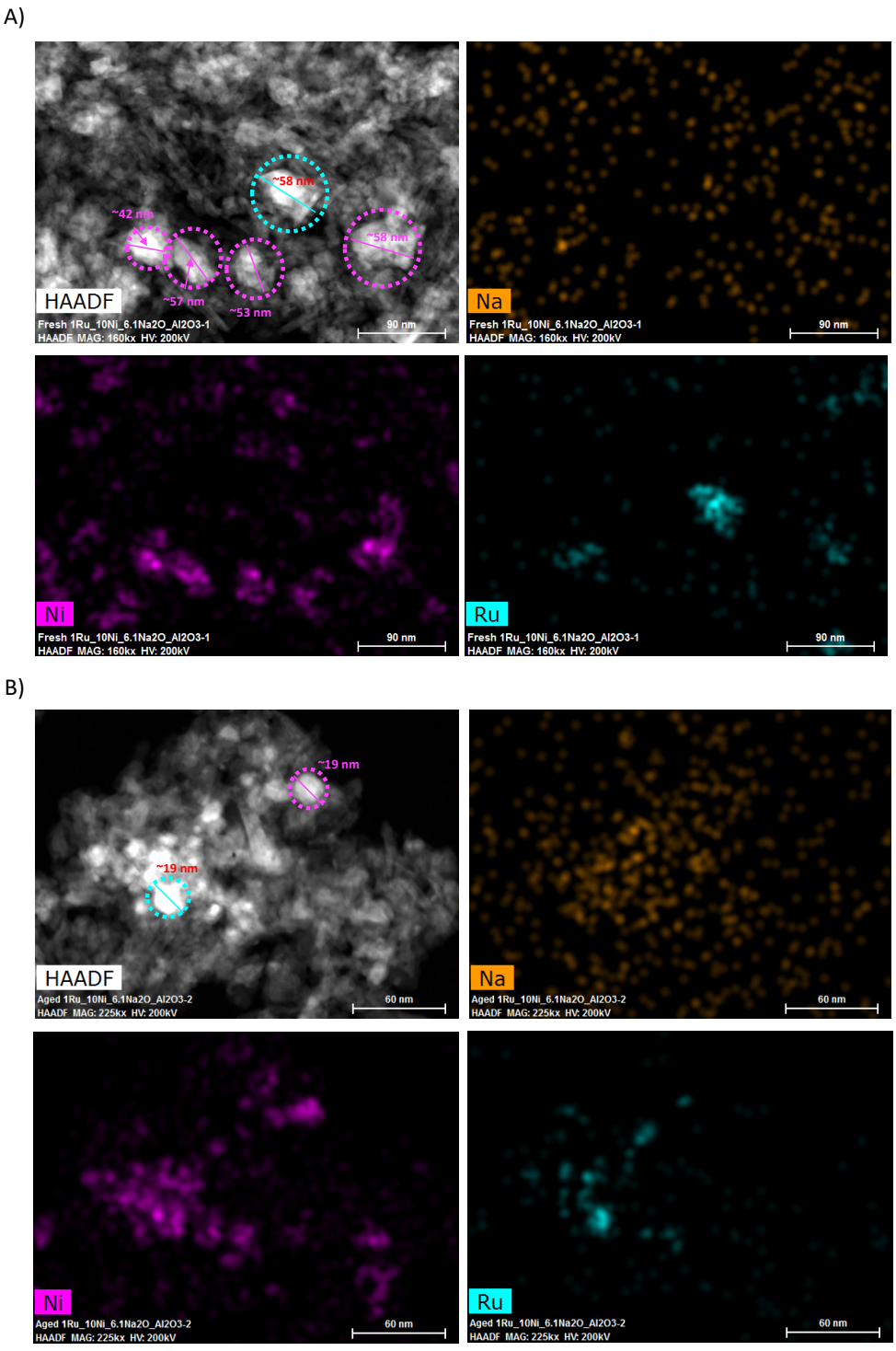

Figure 5.6. STEM-EDS Mapping for A) the fresh and B) aged Ru-doped Ni DFM samples. Areas encircled in light blue are identified as a Ru-rich clusters and areas encircled in pink are identified as Ni-rich clusters with their respective estimated sizes.

Chapter 6: Conclusions and future work

6.1. Thesis conclusion

Several alkaline adsorbents ("Na_2O", CaO, "K_2O" and MgO) were dispersed on Al_2O_3 and tested in combination with 5%Ru. Dispersed "Na_2O" and CaO adsorbents showed the best adsorption capacity but "Na_2O" in concert with Ru, showed the fastest complete conversion of the adsorbed CO_2 towards CH_4 making it the preferred combination. Even though several carriers show a high CO_2 capture capacity, they suffer from poor rates of hydrogenation to CH_4. Al_2O_3 appears to be a preferred DFM carrier when used to support Ru and "Na_2O".

Ruthenium, Rhodium and Nickel incorporated into the DFM (in combination with 6.1% "Na_2O"/Al_2O_3) have been evaluated in simulated O_2 and steam-containing flue gas for hydrogenation rate and quantity of methane production in the DFM process at 320°C and atmospheric pressure. 5% Ruthenium showed the fastest rate with the shortest time for complete methanation. Rhodium was second best for methanation, but its higher cost requires a reduction in metal loading that leads to fewer catalytic sites and lower reaction rates relative to Ru. The Nickel-containing catalysts need to be pre-treated at 650°C with 15%H_2 to reduce NiO to active Ni^0. This produces a very active catalyst, however, methanation could not be achieved at 320°C after O_2 exposure in the capture step, consistent with the capture and conversion steps of DFM, making it unsuitable for the DFM application.

The presence of 1%wt. of Pt or Ru enhance the reduction of NiO_x to metallic Ni (at 320°C) by 50% and 70%, respectively allowing methanation to occur with Ru being the most effective. 1% Ru, 10Ni, 6.1% "Na_2O"/Al_2O_3 DFM showed the best results in terms of CO_2 capture (0.52 mmol CO_2/g) and CH_4 produced (0.38 mmol CH_4/g) with proven cyclic stability over 20 cycles.

The presence of Ni in the 1%Ru-containing DFM enhances CO_2 adsorption (27% higher) but decreases the rate of methanation upon the addition of H_2 (60% slower).

Characterization shows a redispersion of the Ru and Ni catalyst sites as evidenced by higher H_2 uptake per gram of sample and smaller particle size in the aged Ru-doped Ni DFM compared to the fresh sample. XRD patterns confirm a disappearance of the NiO and RuO_x peaks and the appearance of Ru^0 and Ni^0 characteristic peaks in the aged sample due to H_2 exposure during methanation. The possibility of replacing some Ru with Ni is worthy of additional studies for possible additional cost reduction.

6.2. Future work

This thesis successfully demonstrated the feasibility of reducing the amount of precious metal loading in our DFMs from 5% to 1% by replacing some Ru with Ni, a more economical base metal catalyst, without sacrificing their CO_2 capture capacity or methane production. The further reduction of the precious metal loading is of vital importance to make DFM more economically attractive. However, there are still many areas of research opportunity to extensively demonstrate the scalability, flexibility and sustainability of DFM technology.

6.2.1. Ru-doped Ni DFM optimization, scalability and further characterization

As discussed in chapter 5, we studied low (0.1%) and high (1%) Ru loadings in concert with 10%Ni as a candidate catalyst system for DFM. Both Ru and Ni loading studies need to be carried out to maximize CO_2 capture capacity and methane production rates.

Further characterization of the Ru-doped Ni system is also needed. *In-situ* FTIR/DRIFTS studies can help elucidate the CO_2 capture mechanism by identifying the intermediate species

involved that permit an enhanced capture capacity of the bimetallic DFM. It was shown that NiO formed during the capture step can enhance the CO_2 capture, by approx. 20%, and thus should be explored for possible reduction of Ru loadings lower that 1%. The intermediate species involved in the mechanism of NiO reduction at lower temperatures in the presence of Ru as well as the CO_2 spillover to active catalytic sites with the intermediate species for CO_2 methanation on the catalyst system could be studied with particular interest. It would also be of great value to study the oxidation state of the metal and any adsorbent, carrier interaction with the bimetallic DFM with the help of XPS.

There is also the challenge of scaling the Ru-doped Ni DFM from powder to pellet or tablet form. In past studies, our research group has tested different preparation methods to produce a uniformly distributed Ru and "Na_2O" tablet. It would now be necessary to uniformly incorporate Ni in the tablet composition with special attention to the order of impregnation of the species, the precursors utilized, as well as the calcination and pre-reduction methodology. Different alumina tablet geometries (tables vs. hollow extrudates) can also be studied in order to enhance pore-diffusion limitations that impact catalyst and/or adsorbent effectiveness.

6.2.2. Assessment of DFM performance for alternative CO_2 sources and products

To date, DFM has been studied mainly at simulated natural gas power plant flue gas conditions. It might be relevant to study the flexibility of our technology for other applications such as CO_2 streams from flue gas from cement plants and breweries or highly diluted sources such as direct air capture of CO_2 from atmospheric air. The goal is to prove the versatility of DFM to capture CO_2 from a wide spectrum of CO_2 concentrations and catalytic conversion to higher-value products like fuels.

The challenge of this task relies on finding the optimum operation conditions to maximize the CO_2 capture capacity while ensuring high conversion rates of DFM. Concentrated CO_2 streams offer the advantage of enhanced CO_2 capture kinetics, but the space velocity of the CO_2 capture step has to be adjusted to match the kinetics of conversion to ensure a continuous process. On the other hand, dilute CO_2 sources like simulated direct air capture conditions are more challenging. Since the kinetics for CO_2 capture are slower, mass transfer effects occur at low CO_2 concentrations. New reactor designs for enhanced turbulence will likely require a compressor system for the feed stream to drive the capture step. Air also contains a large percentage of oxygen (~21%) which can oxidize our catalyst system in a more permanent way than the current 4.5% O_2 in our simulated flue gas experiments.

There is also considerable value is investigating DFM for producing products of higher value than methane such as methanol or higher hydrocarbons. Higher hydrocarbons also require pressurized processes to meet thermodynamic limitations. Another application would be catalytic dry reforming of adsorbed CO_2 on DFM with CH_4 or reverse water gas shift for CO generation for synthesis gas.

6.2.3. Life cycle and economic analysis of DFM

A detailed life cycle analysis of our technology is needed to corroborate the sustainability of our technology. An equally important economic analysis is also in need to assure DFM's viability and future implementation. A feasible supply of renewable H_2 is still a major unknown factor in the application of DFM to power plants.

The variables of interest for the life cycle analysis include the ecological and carbon footprint of all the processes involved in the DFM implementation, from the catalyst, adsorbent

and carrier production processes and the source of hydrogen (from either renewable power or industrial origin) to the end-use of the fuels or chemicals produced with DFM. A comparison of the carbon footprint of the DFM technology with other known CCUS technologies is also of relevance.

For the economic analysis, it is important to calculate and model the capital costs and operating costs associated with DFM implementation for different CO_2 capture scenarios, the price of the raw mateials, the cost of reactants like renewable hydrogen vs the cost of industrial hydrogen and the power requirements for the operation of any heat exchangers, chillers and compressors needed. It is important to consider the different products that can be made using DFM and their market value and demand. The revenues of the sale and distribution of these products could offset any economic burden associated with the implementation of the new technology.

6.2.4. DFM aging in actual flue gas

The most important technical challenge for DFM is to demonstrate and confirm its life in a real natural gas-fueled power plant or other CO_2 generating sources. This is currently a topic of discussion with Susteon, a US based engineering company with whom we are exploring funding sources for a scale up skid mounted pilot plant that can be used at various CO_2 generating sites.

References

1. IEA, Global Energy & CO_2 Status Report 2017, 2017.
2. Intergovernmental Panel on Climate Change, Summary for Policymakers, in: Intergovernmental Panel on Climate Change (Ed.), Clim. Chang. 2014 Mitig. Clim. Chang., Cambridge University Press, Cambridge, 2014: pp. 1–30.
3. Inventys, (n.d.). http://inventysinc.com (accessed March 13, 2019).
4. Climeworks, (n.d.). http://www.climeworks.com (accessed March 15, 2019).
5. Carbon Engineering, (n.d.). https://carbonengineering.com (accessed March 14, 2019).
6. G.T. Rochelle, Amine Scrubbing for CO_2 Capture, *Science*. 325 (2009) 1652–1654.
7. M. Burkhardt, G. Busch, Methanation of hydrogen and carbon dioxide, *Appl. Energy.* 111 (2013) 74–79.
8. P. Panagiotopoulou, Hydrogenation of CO_2 over supported noble metal catalysts, *Appl. Catal. A Gen*. 542 (2017) 63–70.
9. P. Frontera, A. Macario, M. Ferraro, P. Antonucci, Supported Catalysts for CO_2 Methanation: A Review, *Catalysts*. 7 (2017) 59.
10. K. Stangeland, D. Kalai, H. Li, Z. Yu, CO_2 Methanation: The Effect of Catalysts and Reaction Conditions, *Energy Procedia*. 105 (2017) 2022–2027.
11. K. Müller, M. Fleige, F. Rachow, D. Schmeißer, Sabatier based CO_2-methanation of Flue Gas Emitted by Conventional Power Plants, *Energy Procedia*. 40 (2013) 240–248.
12. D. Türks, H. Mena, U. Armbruster, A. Martin, Methanation of CO_2 on Ni/Al_2O_3 in a Structured Fixed-Bed Reactor—A Scale-Up Study, *Catalysts*. 7 (2017) 152.
13. S.J. Davis, N.S. Lewis, M. Shaner, S. Aggarwal, D. Arent, I.L. Azevedo, S.M. Benson, T. Bradley, J. Brouwer, Y.-M. Chiang, C.T.M. Clack, A. Cohen, S. Doig, J. Edmonds, P.

Fennell, C.B. Field, B. Hannegan, B.-M. Hodge, M.I. Hoffert, E. Ingersoll, P. Jaramillo, K.S. Lackner, K.J. Mach, M. Mastrandrea, J. Ogden, P.F. Peterson, D.L. Sanchez, D. Sperling, J. Stagner, J.E. Trancik, C.-J. Yang, K. Caldeira, Net-zero emissions energy systems, *Science*. 360 (2018) eaas9793.

14. G. Glenk, S. Reichelstein, Economics of converting renewable power to hydrogen, *Nat. Energy*. 4 (2019) 216–222.

15. M.S. Duyar, M.A. Arellano-Treviño, R.J. Farrauto, Dual function materials for CO_2 capture and conversion using renewable H_2, *Appl. Catal. B Environ*. 168–169 (2015) 370–376.

16. P. Gruene, A.G. Belova, T.M. Yegulalp, R.J. Farrauto, M.J. Castaldi, Dispersed Calcium Oxide as a Reversible and Efficient CO_2 −Sorbent at Intermediate Temperatures, *Ind. Eng. Chem. Res*. 50 (2011) 4042–4049.

17. L. Proaño, E. Tello, M.A. Arellano-Trevino, S. Wang, R.J. Farrauto, M. Cobo, In-situ DRIFTS study of two-step CO_2 capture and catalytic methanation over Ru,"Na_2O"/Al_2O_3 Dual Functional Material, *Appl. Surf. Sci.* 479 (2019) 25–30.

18. S. Wang, R.J. Farrauto, S. Karp, J.H. Jeon, E.T. Schrunk, Parametric, cyclic aging and characterization studies for CO_2 capture from flue gas and catalytic conversion to synthetic natural gas using a dual functional material (DFM), *J. CO_2 Util.* 27 (2018) 390–397.

19. S. Wang, E.T. Schrunk, H. Mahajan, and R.J. Farrauto, The Role of Ruthenium in CO_2 Capture and Catalytic Conversion to Fuel by Dual Function Materials (DFM), *Catalysts*. 7 (2017) 88.

20. Q. Zheng, R. Farrauto, A. Chau Nguyen, Adsorption and Methanation of Flue Gas CO_2

with Dual Functional Catalytic Materials: A Parametric Study, *Ind. Eng. Chem. Res*. 55 (2016) 6768–6776.

21. M.S. Duyar, S. Wang, M.A. Arellano-Treviño, R.J. Farrauto, CO_2 utilization with a novel dual function material (DFM) for capture and catalytic conversion to synthetic natural gas: An update, *J. CO_2 Util.* 15 (2016) 65–71.

22. M. Mihet, M.D. Lazar, Methanation of CO_2 on Ni/γ-Al_2O_3: Influence of Pt, Pd or Rh promotion, *Catal. Today*. 306 (2018) 294–299.

23. IPCC, Chapter 1 Framing and Context, Glob. Warm. 1.5°C. An IPCC Spec. Rep. Impacts Glob. Warm. 1.5°C above Pre-Industrial Levels Relat. Glob. Greenh. Gas Emiss. Pathways, Context Strength. Glob. Response to Threat Clim. Chang. (2018).

24. Y. Chen, B. Li, Z. Li, X. Shi, Quantitatively evaluating the effects of CO_2 emission on temperature rise, *Quat. Int.* 336 (2014) 171–175.

25. E.D. and P. Tans, NOAA/ESRL, (n.d.). https://www.esrl.noaa.gov/gmd/ccgg/trends/global.html (accessed July 18, 2019).

26. J.H. Butler, S.A. Montzka, The NOAA Annual Greenhouse Gas Index (AGGI), NOAA/ESRL. (2019). https://www.esrl.noaa.gov/gmd/aggi/aggi.html (accessed July 19, 2019).

27. P. Tans, Monthly Mean Carbon Dioxide, NOAA ESRL Carbon Cycle. (n.d.). https://www.esrl.noaa.gov/gmd/ccgg/gallery/figures/pdf/co2_mm_obs.pdf (accessed July 18, 2019).

28. M.S. Duyar, R.J. Farrauto, M.J. Castaldi, T.M. Yegulalp, In Situ CO_2 Capture Using CaO/γ-Al_2O_3 Washcoated Monoliths for Sorption Enhanced Water Gas Shift Reaction, *Ind. Eng. Chem. Res*. 53 (2014) 1064–1072.

29. K.B. Lee, M.G. Beaver, H.S. Caram, S. Sircar, Reversible chemisorption of carbon dioxide: Simultaneous production of fuel-cell grade H_2 and compressed CO_2 from synthesis gas, *Adsorption*. 13 (2007) 385–397.

30. R.M. Cuéllar-Franca, A. Azapagic, Carbon capture, storage and utilisation technologies: A critical analysis and comparison of their life cycle environmental impacts, *J. CO_2 Util.* 9 (2015) 82–102.

31. D.Y.C. Leung, G. Caramanna, M.M. Maroto-Valer, An overview of current status of carbon dioxide capture and storage technologies, *Renew. Sustain. Energy Rev*. 39 (2014) 426–443.

32. D.W. Keith, Why Capture CO_2 from the Atmosphere?, *Science.* 325 (2009) 1654 – 1655.

33. M. Fasihi, O. Efimova, C. Breyer, Techno-economic assessment of CO_2 direct air capture plants, *J. Clean. Prod.* 224 (2019) 957–980.

34. D.W. Keith, G. Holmes, D. St. Angelo, K. Heidel, A Process for Capturing CO_2 from the Atmosphere, *Joule*. 2 (2018) 1573–1594.

35. J. V. Veselovskaya, V.S. Derevschikov, T.Y. Kardash, A.G. Okunev, Direct CO_2 capture from ambient air by K_2CO_3 / alumina composite sorbent for synthesis of renewable methane, *Renew. Bioresour*. 3 (2015) 1–7.

36. J. V Veselovskaya, P.D. Parunin, A.G. Okunev, Catalytic process for methane production from atmospheric carbon dioxide utilizing renewable energy, *Catal. Today.* 298 (2017) 117–123.

37. J. V. Veselovskaya, P.D. Parunin, O. V. Netskina, A.G. Okunev, A Novel Process for Renewable Methane Production: Combining Direct Air Capture by K_2CO_3/Alumina Sorbent with CO_2 Methanation over Ru/Alumina Catalyst, *Top. Catal*. 0 (2018) 1–9.

38. C.H. Bartholomew, R.J. Farrauto, Fundamentals of Industrial Catalytic Processes, John Wiley & Sons, Inc., Hoboken, NJ, USA, 2005.

39. C.H. Yu, C.H. Huang, C.S. Tan, A Review of CO_2 Capture by Absorption and Adsorption, *Aerosol Air Qual. Res*. 12 (2012) 745–769.

40. P. Luis, Use of monoethanolamine (MEA) for CO_2 capture in a global scenario: Consequences and alternatives, *Desalination.* 380 (2016) 93–99.

41. A. Samanta, A. Zhao, G.K.H. Shimizu, P. Sarkar, R. Gupta, Post-Combustion CO_2 Capture Using Solid Sorbents: A Review, *Ind. Eng. Chem. Res*. 51 (2012) 1438–1463.

42. Y. Wang, L. Zhao, A. Otto, M. Robinius, D. Stolten, A Review of Post-combustion CO_2 Capture Technologies from Coal-fired Power Plants, *Energy Procedia*. 114 (2017) 650–665.

43. J.D. Figueroa, T. Fout, S. Plasynski, H. McIlvried, R.D. Srivastava, Advances in CO_2 capture technology—The U.S. Department of Energy's Carbon Sequestration Program, *Int. J. Greenh. Gas Control*. 2 (2008) 9–20.

44. B.J. Maring, P.A. Webley, A new simplified pressure/vacuum swing adsorption model for rapid adsorbent screening for CO_2 capture applications, *Int. J. Greenh. Gas Control*. 15 (2013) 16–31.

45. K.B. Lee, M.G. Beaver, H.S. Caram, S. Sircar, Reversible chemisorbents for carbon dioxide and their potentail applications, *Ind. Eng. Chem. Res*. 47 (2008) 8048–8062.

46. W. Wang, S. Wang, X. Ma, J. Gong, Recent advances in catalytic hydrogenation of carbon dioxide., *Chem. Soc. Rev*. 40 (2011) 3703–27.

47. H. Luo, H. Kanoh, Fundamentals in CO_2 capture of Na_2CO_3 under a moist condition, *J. Energy Chem.* 26 (2017) 972–983.

48. A. Al-Mamoori, H. Thakkar, X. Li, A.A. Rownaghi, F. Rezaei, Development of Potassium- and Sodium-Promoted CaO Adsorbents for CO_2 Capture at High Temperatures, *Ind. Eng. Chem. Res*. 56 (2017) 8292–8300.

49. A. Al-Mamoori, S. Lawson, A. A. Rownaghi, F. Rezaei, Improving Adsorptive Performance of CaO for High-Temperature CO_2 Capture through Fe and Ga Doping, *Energy & Fuels*. 33 (2019) 1404–1413.

50. Y.-J. Wu, P. Li, J.-G. Yu, A.F. Cunha, A.E. Rodrigues, Progress on sorption-enhanced reaction process for hydrogen production, *Rev. Chem. Eng.* 32 (2016) 271.

51. S.C. Lee, B.Y. Choi, T.J. Lee, C.K. Ryu, Y.S. Ahn, J.C. Kim, CO_2 absorption and regeneration of alkali metal-based solid sorbents, *Catal. Today*. 111 (2006) 385–390.

52. K.B. Lee, M.G. Beaver, H.S. Caram, S. Sircar, Chemisorption of carbon dioxide on sodium oxide promoted alumina, *AIChE J*. 53 (2007) 2824–2831.

53. T.S. Nguyen, L. Lefferts, K.B. Saisankargupta, K. Seshan, Catalytic Conversion of Biomass Pyrolysis Vapours over Sodium-Based Catalyst: A Study on the State of Sodium on the Catalyst, *ChemCatChem*. 7 (2015) 1833–1840.

54. C.J. Keturakis, F. Ni, M. Spicer, M.G. Beaver, H.S. Caram, I.E. Wachs, Monitoring solid oxide CO_2 capture sorbents in action, *ChemSusChem*. 7 (2014) 3459–3466.

55. J.Q. Shi, S. Durucan, CO_2 storage in deep unminable coal seams, *Oil Gas Sci. Technol.* 60 (2005) 547–558.

56. V. Rai, N.-C. Chung, M.C. Thurber, D.G. Victor, PESD Carbon Storage Project Database, *SSRN Electron. J.* (2008).

57. C.M. White, D.H. Smith, K.L. Jones, A.L. Goodman, S.A. Jikich, R.B. LaCount, S.B. DuBose, E. Ozdemir, B.I. Morsi, K.T. Schroeder, Sequestration of Carbon Dioxide in

Coal with Enhanced Coalbed Methane Recovery: A Review, *Energy & Fuels*. 19 (2005) 659–724.

58. S. Garcia, S. Kaminska, M. Mercedes Maroto-Valer, Underground carbon dioxide storage in saline formations, *Proc. Inst. Civ. Eng. - Waste Resour. Manag*. 163 (2010) 77–88.

59. E.I. Koytsoumpa, C. Bergins, E. Kakaras, The CO_2 economy: Review of CO_2 capture and reuse technologies, *J. Supercrit. Fluids*. 132 (2018) 3–16.

60. E. Alper, O. Yuksel Orhan, CO_2 utilization: Developments in conversion processes, *Petroleum*. 3 (2017) 109–126.

61. B. Wang, Y. Li, N. Wu, C.Q. Lan, CO_2 bio-mitigation using microalgae, *Appl. Microbiol. Biotechnol.* 79 (2008) 707–718.

62. T.M. Mata, A.A. Martins, N.S. Caetano, Microalgae for biodiesel production and other applications: A review, *Renew. Sustain. Energy Rev*. 14 (2010) 217–232.

63. Y. Qin, X. Sheng, S. Liu, G. Ren, X. Wang, F. Wang, Recent advances in carbon dioxide based copolymers, *J. CO_2 Util*. 11 (2015) 3–9.

64. B. Hu, C. Guild, S.L. Suib, Thermal, electrochemical, and photochemical conversion of CO_2 to fuels and value-added products, *J. CO2 Util*. 1 (2013) 18–27.

65. K.P. Yu, W.Y. Yu, M.C. Kuo, Y.C. Liou, S.-H. Chien, Pt/titania-nanotube: A potential catalyst for CO_2 adsorption and hydrogenation, *Appl. Catal. B Environ*. 84 (2008) 112–118.

66. D.T. Whipple, P.J.A. Kenis, Prospects of CO_2 Utilization via Direct Heterogeneous Electrochemical Reduction, *J. Phys. Chem. Lett.* 1 (2010) 3451–3458.

67. M. Pérez-Fortes, J.C. Schöneberger, A. Boulamanti, G. Harrison, E. Tzimas, Formic acid

synthesis using CO_2 as raw material: Techno-economic and environmental evaluation and market potential, *Int. J. Hydrogen Energy*. 41 (2016) 16444–16462.

68. M. Pérez-Fortes, J.C. Schöneberger, A. Boulamanti, E. Tzimas, Methanol synthesis using captured CO_2 as raw material: Techno-economic and environmental assessment, *Appl. Energy*. 161 (2016) 718–732.

69. C. Janke, M.S. Duyar, M. Hoskins, R. Farrauto, Catalytic and adsorption studies for the hydrogenation of CO_2 to methane, *Appl. Catal. B Environ*. 152–153 (2014) 184–191.

70. M. Götz, J. Lefebvre, F. Mörs, A. McDaniel Koch, F. Graf, S. Bajohr, R. Reimert, T. Kolb, Renewable Power-to-Gas: A technological and economic review, *Renew. Energy*. 85 (2016) 1371–1390.

71. S. Schiebahn, T. Grube, M. Robinius, V. Tietze, B. Kumar, D. Stolten, Power to gas: Technological overview, systems analysis and economic assessment for a case study in Germany, *Int. J. Hydrogen Energy*. 40 (2015) 4285–4294.

72. K. Stangeland, D. Kalai, H. Li, Z. Yu, CO_2 methanation: the effect of catalysts and reaction conditions, *Energy Procedia*. 105 (2017) 2022–2027.

73. A. Wo, P. Ruiz, M. Jacquemin, Catalytic CO_2 methanation process, US Patent WO2010006386A2. 2010..

74. W. Wei, G. Jinlong, Methanation of carbon dioxide: an overview, Front. *Chem. Sci. Eng*. 5 (2010) 2–10.

75. T. Vanherwijnen, Kinetics of the methanation of CO and CO_2 on a nickel catalyst, *J. Catal*. 28 (1973) 391–402.

76. G. Garbarino, P. Riani, L. Magistri, G. Busca, A study of the methanation of carbon dioxide on Ni/Al_2O_3 catalysts at atmospheric pressure, *Int. J. Hydrogen Energy*. 39

(2014) 11557–11565.

77. G. Garbarino, D. Bellotti, P. Riani, L. Magistri, G. Busca, Methanation of carbon dioxide on Ru/Al_2O_3 and Ni/Al_2O_3 catalysts at atmospheric pressure: Catalysts activation, behaviour and stability, *Int. J. Hydrogen Energy*. 40 (2015) 9171–9182.

78. F. Solymosi, A. Erdöhelyi, Methanation of CO_2 on Supported Rhodium Catalysts, *Stud. Surf. Sci. Catal*. 7 (1981) 1448–1449.

79. F. Solymosi, A. Erdöhelyi, Hydrogenation of CO_2 to CH_4 over alumina-supported noble metals, *J. Mol. Catal.* 8 (1980) 471–474.

80. A. Erdohelyi, Catalytic hydrogenation of CO_2 over supported palladium, *J. Catal*. 98 (1986) 166–177.

81. K. Müller, M. Fleige, F. Rachow, D. Schmeißer, Sabatier based CO_2-methanation of flue gas emitted by conventional power plants, *Energy Procedia*, 40 (2013) 240–248.

82. H. Muroyama, Y. Tsuda, T. Asakoshi, H. Masitah, T. Okanishi, T. Matsui, K. Eguchi, Carbon dioxide methanation over Ni catalysts supported on various metal oxides, *J. Catal*. 343 (2016) 178–184.

83. G. Garbarino, D. Bellotti, E. Finocchio, L. Magistri, G. Busca, Methanation of carbon dioxide on Ru/Al_2O_3: Catalytic activity and infrared study, *Catal. Today*. 277 (2016) 21–28.

84. H. Muroyama, Y. Tsuda, T. Asakoshi, H. Masitah, T. Okanishi, T. Matsui, K. Eguchi, Carbon dioxide methanation over Ni catalysts supported on various metal oxides, *J. Catal.* 343 (2016) 178–184.

85. C. Fukuhara, K. Hayakawa, Y. Suzuki, W. Kawasaki, R. Watanabe, A novel nickel-based structured catalyst for CO_2 methanation: A honeycomb-type Ni/CeO_2 catalyst to

transform greenhouse gas into useful resources, Appl. Catal. A Gen. 532 (2017) 12–18.

86. S. Rahmani, M. Rezaei, F. Meshkani, Preparation of promoted nickel catalysts supported on mesoporous nanocrystalline gamma alumina for carbon dioxide methanation reaction, *J. Ind. Eng. Chem*. 20 (2014) 4176–4182.

87. J.A.H. Dreyer, P. Li, L. Zhang, G.K. Beh, R. Zhang, P.H.L. Sit, W.Y. Teoh, Influence of the oxide support reducibility on the CO_2 methanation over Ru-based catalysts, *Appl. Catal. B Environ*. 219 (2017) 715–726.

88. J.M. Rynkowski, T. Paryjczak, A. Lewicki, M.I. Szynkowska, T.P. Maniecki, W.K. Jóźwiak, Characterization of Ru/CeO_2-Al_2O_3 catalysts and their Performance in CO_2 Methanation, *React. Kinet. Catal. Lett*. 71 (2000) 55–64.

89. S. Sharma, Z. Hu, P. Zhang, E.W. McFarland, H. Metiu, CO_2 methanation on Ru-doped ceria, *J. Catal*. 278 (2011) 297–309.

90. Q. Pan, J. Peng, T. Sun, S. Wang, S. Wang, Insight into the reaction route of CO_2 methanation: Promotion effect of medium basic sites, *Catal. Commun*. 45 (2014) 74–78.

91. I. Graça, L. V. González, M.C. Bacariza, A. Fernandes, C. Henriques, J.M. Lopes, M.F. Ribeiro, CO_2 hydrogenation into CH_4 on NiHNaUSY zeolites, *Appl. Catal. B Environ*. 147 (2014) 101–110.

92. M.C. Bacariza, I. Graça, J.M. Lopes, C. Henriques, Enhanced activity of CO_2 hydrogenation to CH_4 over Ni based zeolites through the optimization of the Si/Al ratio, *Microporous Mesoporous Mater*. 267 (2018) 9–19.

93. M.C. Bacariza, M. Maleval, I. Graça, J.M. Lopes, C. Henriques, Power-to-methane over Ni/zeolites: Influence of the framework type, *Microporous Mesoporous Mater*. 274 (2019) 102–112.

94. M.C. Bacariza, I. Graça, J.M. Lopes, C. Henriques, Ni-Ce/Zeolites for CO_2 Hydrogenation to CH_4: Effect of the Metal Incorporation Order, *ChemCatChem.* 10 (2018) 2773–2781.

95. K. Kitamura Bando, K. Soga, K. Kunimori, H. Arakawa, Effect of Li additive on CO_2 hydrogenation reactivity of zeolite supported Rh catalysts, *Appl. Catal. A Gen*. 175 (1998) 67–81.

96. A. Kim, D.P. Debecker, F. Devred, V. Dubois, C. Sanchez, C. Sassoye, CO_2 methanation on Ru/TiO_2 catalysts: On the effect of mixing anatase and rutile TiO_2 supports, *Appl. Catal. B Environ*. 220 (2018) 615–625.

97. Q. Lin, X.Y. Liu, Y. Jiang, Y. Wang, Y. Huang, T. Zhang, Crystal phase effects on the structure and performance of ruthenium nanoparticles for CO_2 hydrogenation, *Catal. Sci. Technol*. 4 (2014) 2058–2063.

98. M.E.T. Al, The Location Catalysts : of Nickel Oxide and Nickel in Silica-Supported Two Forms of " NiO " and the Assignment of Reduction Profiles, *J. Catal*. 229 (1988) 217–229.

99. R. Bal, B.B. Tope, T.K. Das, S.G. Hegde, S. Sivasanker, Alkali-loaded silica, a solid base: Investigation by FTIR spectroscopy of adsorbed CO_2 and its catalytic activity, *J. Catal*. 204 (2001) 358–363.

100. J. Polanski, T. Siudyga, P. Bartczak, M. Kapkowski, W. Ambrozkiewicz, A. Nobis, R. Sitko, J. Klimontko, J. Szade, J. Lelątko, Oxide passivated Ni-supported Ru nanoparticles in silica: A new catalyst for low-temperature carbon dioxide methanation, *Appl. Catal. B Environ*. 206 (2017) 16–23.

101. G. Zhou, T. Wu, H. Xie, X. Zheng, Effects of structure on the carbon dioxide

methanation performance of Co-based catalysts, *Int. J. Hydrogen Energy*. 38 (2013) 10012–10018.

102. C. V. Miguel, M.A. Soria, A. Mendes, L.M. Madeira, A sorptive reactor for CO_2 capture and conversion to renewable methane, *Chem. Eng. J*. 322 (2017) 590–602.

103. S.M. Kim, P.M. Abdala, M. Broda, D. Hosseini, C. Copéret, C. Müller, Integrated CO_2 Capture and Conversion as an Efficient Process for Fuels from Greenhouse Gases, *ACS Catal*. 8 (2018) 2815–2823.

104. H. Sun, J. Wang, J. Zhao, B. Shen, J. Shi, J. Huang, C. Wu, Dual functional catalytic materials of Ni over Ce-modified CaO sorbents for integrated CO_2 capture and conversion, *Appl. Catal. B Environ*. 244 (2019) 63–75.

105. A. Al-Mamoori, A.A. Rownaghi, F. Rezaei, Combined Capture and Utilization of CO_2 for Syngas Production over Dual-Function Materials, *ACS Sustain. Chem. Eng.* 6 (2018) 13551–13561.

106. F. Drault, C. Comminges, F. Can, L. Pirault-Roy, F. Epron, A. Le Valant, Palladium, Iridium, and Rhodium Supported Catalysts: Predictive H_2 Chemisorption by Statistical Cuboctahedron Clusters Model, *Materials*. 11 (2018) 819.

107. L. Shore, W.F. Ruettinger, R.J. Farrauto, Platinum gropu metal promoted copper oxidation catalysts and methods for carbon monoxide remediation, US006913739BS, 2005.

108. Q. Zhang, L. Shore, R.J. Farrauto, Selective CO oxidation over a commercial PROX monolith catalyst for hydrogen fuel cell applications, *Int. J. Hydrogen Energy*. 37 (2012) 10874–10880.

109. M.A.A. Aziz, A.A. Jalil, S. Triwahyono, S.M. Sidik, Applied Catalysis A : General

Methanation of carbon dioxide on metal-promoted mesostructured silica nanoparticles, *Applied Catal. A, Gen.* 486 (2014) 115–122.

110. W. Yu, M.D. Porosoff, J.G. Chen, Review of Pt-Based Bimetallic Catalysis: From Model Surfaces to Supported Catalysts, *Chem. Rev*. 112 (2012) 5780–5817.

111. W. Zhen, B. Li, G. Lu, J. Ma, Enhancing catalytic activity and stability for CO_2 methanation on Ni–Ru/γ-Al_2O_3 via modulating impregnation sequence and controlling surface active species, *RSC Adv*. 4 (2014) 16472–16479.

112. A. Tsuneto, A. Kudo, N. Saito, T. Sakata, Hydrogenation of Solid State Carbonates, *Chem. Lett*. 21 (1992) 831–834.

113. L. He, Q. Lin, Y. Liu, Y. Huang, Unique catalysis of Ni-Al hydrotalcite derived catalyst in CO_2 methanation: Cooperative effect between Ni nanoparticles and a basic support, *J. Energy Chem*. 23 (2014) 587–592.

114. J. Guo, Z. Hou, J. Gao, X. Zheng, DRIFTS Study on Adsorption and Activation of CH_4 and CO_2 over Ni/SiO_2 Catalyst with Various Ni Particle Sizes, *Chinese J. Catal*. 28 (2007) 22–26.

115. B. Mutz, H.W.P. Carvalho, S. Mangold, W. Kleist, J.D. Grunwaldt, Methanation of CO_2: Structural response of a Ni-based catalyst under fluctuating reaction conditions unraveled by operando spectroscopy, *J. Catal*. 327 (2015) 48–53.

116. B. Mutz, A. Gänzler, M. Nachtegaal, O. Müller, R. Frahm, W. Kleist, J.-D. Grunwaldt, Surface Oxidation of Supported Ni Particles and Its Impact on the Catalytic Performance during Dynamically Operated Methanation of CO_2, *Catalysts*. 7 (2017) 279.

117. K. Aika, A. Ohya, A. Ozaki, Y. Inoue, I. Yasumori, Support and promoter effect of ruthenium catalyst. II. Ruthenium/alkaline earth catalyst for activation of dinitrogen, *J.*

Catal. 92 (1985) 305–311.

118. A. Petala, P. Panagiotopoulou, Methanation of CO_2 over alkali-promoted Ru/TiO_2 catalysts: Effect of alkali additives on catalytic activity and selectivity, *Appl. Catal. B Environ*. 224 (2018) 919–927.

119. D.J.C. Yates, J.H. Sinfelt, The catalytic activity of rhodium in relation to its state of dispersion, *J. Catal*. 8 (1967) 348–358.

120. L. Li, X. Wen, X. Fu, F. Wang, N. Zhao, F. Xiao, W. Wei, Y. Sun, MgO/Al_2O_3 Sorbent for CO_2 Capture, *Energy & Fuels*. 24 (2010) 5773–5780.

121. H.A. Al-Madfaa, M.M. Khader, Reduction kinetics of ceria surface by hydrogen, *Mater. Chem. Phys*. 86 (2004) 180–188.

122. T. Matsukawa, A.H. and T. Ishigaki, Temperature-induced structural transition of ceria by bulk reduction under hydrogen atmosphere, *CrystEngComm*. 20 (2018) 4359–4363.

123. M.A. Arellano-Treviño, Z. He, M.C. Libby, R.J. Farrauto, Catalysts and adsorbents for CO_2 capture and conversion with dual function materials: Limitations of Ni-containing DFMs for flue gas applications, *J. CO_2 Util.* 31 (2019) 143–151.

124. A. Ueno, J.K. Hochmuth, C.O. Bennett, Interaction of CO_2, CO, and NiO studied by infrared spectroscopy, *J. Catal*. 49 (1977) 225–235.